



ebn



Exploring electrofacies for property mapping of the Triassic: an improved approach for geothermal development in Brabant.

Ellen Peereboom
Utrecht University

Master's thesis | Earth Structure and Dynamics | October 2018

Supervisors: Jan Lutgert (EBN B.V.) and Dr. W.W.W. Beekman (Utrecht University)

Student no. 3817717 | ellenpeereboom@gmail.com

Abstract

Geothermal energy in the Netherlands has been receiving increased attention recently since it may be a promising contributor to the energy transition. Public well data that has been acquired for hydrocarbon exploration can now be used to assess the potential of geothermal plays. Similarly to hydrocarbon reservoirs, the reservoir quality of a geothermal play is largely controlled by three factors: facies, maximum burial depth and diagenesis. The direct onset for this project has been the release of the regional property maps by TNO, 2017. The aim of this study was to improve the methodology for property maps of the Triassic formations from the Roer Valley Graben in Noord-Brabant, SE Netherlands. The approach has been twofold by (1) a detailed analysis of the current mapping methodologies and their limitations, followed by (2) a lithology prediction analysis as an addition to the existing workflow. In previous studies, regional porosity maps have been made for the West Netherlands Basin (Vis et al., 2010) and for the entire Netherlands (including offshore) in 2017. Both mapping projects were based on porosity data from wells, although different driving maps have been used; respectively facies and maximum burial depth.

Given the strong relation between maximum burial depth and provenance, the maximum-burial driven maps provide a good indication for regional property trends. However, this relation is not valid for individual wells, hence neither in local geothermal enterprises. Given the heterogeneous nature of e.g. a braided channel complex, a local geological lithofacies interpretation is required. The facies-driven property maps as constructed for the West Netherlands Basin use lateral extrapolation of facies modelling and assign porosity values to each facies. Due to the sparse amount of data available and related loss of detail and oversimplification this method is not preferred for the Roer Valley Graben.

To improve the current mapping methodology, our knowledge of the wells should be enhanced first. Therefore lithology characterization and prediction have been explored. The workflow starts with the use of cluster analysis of interpreted facies intervals. Cluster analysis has been performed by *Wkmeans* on intervals of three wells within the area: KDK-01, WWK-01 and WWS-01-S1. Since lithology prediction is not possible with this tool, this method requires further development. Lithology prediction has been performed in *Petrel* on intervals of three wells within the area: BRAK-01, KDK-01 and WWN-01-S2. The input consisted of lithofacies interpretations, followed by either of the two classification techniques: a Bayes classifier and a neural network. The classification based on Bayes algorithm generally yielded poor, discontinuous lithofacies logs. The poor results were mostly due to insufficient input data, e.g. only 1 interval with a distinct lithofacies. Lithology predictions with a neural net created good lithofacies logs. Cross-checks within the wells validated the fairly good results. Wireline logs (e.g. GR, RHOB, RT) resulted in continuous lithofacies logs, whereas core plug logs (porosity, horizontal permeability, grain density) resulted in discontinuous lithofacies logs. Furthermore sufficiently long intervals with separate facies intervals drastically improve the lithology prediction.

The neural net classifier has proven to be a promising technique to validate and predict lithofacies within a well. The lateral extension to other wells should be approached with caution, at least for this particular dataset. Since a large number of logs and interpretations will yield the best predictions, the need for extensive, full-range data acquisition is emphasized. Finally, this study also stresses that the intended users of regional property maps should become well-informed on the uncertainties related to the making of these maps.

Index

Abstract	3
1. Introduction	6
2. Geological setting	7
2.1 Geological evolution	7
2.1.1 Paleozoic	7
2.1.2 Permian	7
2.1.3 Triassic	7
2.2 Tectonic evolution	8
2.3 Structural elements & stratigraphy	9
3. Petrophysical background	10
3.1 Facies	11
3.2 Burial	12
3.3 Diagenesis	12
4. Methods	13
4.1 Data handling / selection	13
4.2 Log interpretation	13
4.3 Electrofacies modelling	14
4.3.1 Cluster analysis in Wkmeans	15
4.3.2 Lithology prediction in Petrel	15
5. Results	18
5.1 Controls on Reservoir Quality	18
5.1.1 Facies	18
5.1.2 Burial	Fout! Bladwijzer niet gedefinieerd.
5.1.3 Diagenesis	19
5.2 Cluster analysis in Wkmeans	20
5.2.1 BRAK-01	20
5.2.2 KDK-01	23
5.2.3 WWK-01	26
5.2.4 WWS-01-S1	28
5.3 Lithology prediction in Petrel	30
5.3.1 BRAK-01	30
5.3.2 KDK-01	31
5.3.3 WWN-01-S2	33
6. Discussion	34
6.1 Cluster analysis in Wkmeans	34
6.1.1 BRAK-01	34
6.1.2 KDK-01	34
6.1.3 WWK-01	34
6.1.4 WWS-01-S1	34
6.2 Lithology prediction in Petrel	35
6.2.1 BRAK-01	35
6.2.2 KDK-01	35
6.2.3 WWN-01-S2	35

6.3	Property maps	36
6.3.1	<i>Maximum Burial driven</i>	36
6.3.2	<i>Facies driven</i>	37
6.3.3	<i>Exploring electrofacies</i>	37
7.	Conclusions	39
8.	Recommendations	40
9.	Acknowledgements.....	41
10.	References	42
	Appendix I: Glossary/Index	44
	Appendix II: Depositional environments.....	45
	BRAK-01.....	45
	KDK-01.....	46
	WWN-01-S2.....	46
	Appendix III: Results Lithoclassification Petrel.....	48
	Probability density functions (PDFs).....	48
	<i>BRAK-01</i>	48
	<i>KDK-01</i> 49	
	<i>WWN-01-S2</i>	49
	Poroperms & porosity-depth plots.....	50
	<i>BRAK-01</i>	50
	<i>KDK-01</i> 51	
	<i>WWN-01-S2</i>	52
	Appendix IV: Well sections.....	53
	BRAK-01.....	53
	KDK-01.....	55
	WWK-01	57
	WWN-01-S2.....	58
	WWS-01-S1	59

1. Introduction

Due to the induced seismicity in the Groningen gas field, the need for speeding up the energy transition in the Netherlands becomes clear. Geothermal energy production from the Dutch subsurface is one of the options to contribute to this transition.

Onset of this thesis is the property maps project performed by TNO in 2017, which resulted in porosity and permeability (i.e. properties) maps of 19 horizons of the Dutch subsurface. Porosity and permeability measurements were either measured directly or calculated via other measurements. Statistical methods allowed the properties determined from the well, as points on the map, to be interpolated and extrapolated laterally to create a surface. However, careful investigation of the initial data showed a number of discrepancies with the presented property values. In several wells, there is a misfit between the core plugs and log data, and often only the upper part of the interval is sampled for plugs. It often appears this upper part is not entirely representative for the complete interval, which may result in overly optimistic or pessimistic predictions of reservoir quality. These observations and implications demonstrate the need for a thorough re-examination of the basic assumptions and methodology of the property maps.

The study area is located in Noord-Brabant or the Roer Valley Graben and the focus lies on the Triassic formations. Aquifer temperatures in large parts of the area are the highest of all Triassic formations in the Netherlands (Bonté et al., 2012) and geothermal doublets have been estimated to produce sufficient power potential (Kramers et al., 2012). Combined with the large heat demand from the local industry, East Brabant is a major geothermal target for the Netherlands.

Therefore the main controls on reservoir quality will be explored. The facies, diagenesis and maximum burial are all known to influence the porosity and permeability of a reservoir.

Previous work by TNO has resulted in porosity maps based on maximum burial depth. Moreover the classical facies-upscaling approach has been applied for several areas, e.g. the West Netherlands basin (Vis et al., 2010). In order to present a more reasonable regional impression of the properties of the Triassic Brabant, both the regional and local geology of Brabant has to be taken into account, rather than a mere statistical approach. A combination of geostatistics within a well and geological lateral extrapolation based on lithofacies is explored here.

The project objective of this thesis is to improve the methodology behind the property maps of the Triassic formations of East Brabant. It must be noted that this project is not meant as a mapping exercise but rather provides a detailed analysis of the current methodologies behind the creation of these maps, as well as a means of introducing an additional geostatistical analysis into the workflow.

The research questions are formulated as follows: What are the current limitations of the property map methodology? How could the property maps be improved?

2. Geological setting

Here a concise geological history on the Dutch subsurface is presented, with particular focus on the development of the Permian and Triassic basins which would evolve to become important reservoirs, one of which is the Roer Valley Graben in Brabant. Numerous studies have been carried out over the past decades to determine the hydrocarbon storage potential of these reservoirs, but the same understanding can now be used to explore the possibilities of geothermal exploitation. The tectonics that shaped the basement, the sediment type and derived depositional environment and the tectonics post-deposition will be discussed.

2.1 Geological evolution

2.1.1 Paleozoic

The paleoposition of the Netherlands during the Late Ordovician (458 Ma) was on the continent Avalonia at 60 degrees latitude on the southern hemisphere. Collision of the northward drifting Avalonia with the larger Laurentia and Baltica during the Silurian (433 Ma) caused the Caledonian orogeny. This new assembled continent was known as Laurussia, which in turn collided with Gondwana during the Early Carboniferous (342 Ma), at which time the Netherlands was located at the equator. The collision of Laurussia and Gondwana resulted in the birth of supercontinent Pangea, an event that was accompanied by another phase of large-scale mountain building (Variscan or Hercynian orogeny) and subsequent magmatic events (de Jager, 2007). By the Late Carboniferous (300 Ma), the Netherlands was located in the central part of Pangea and north of the E-W striking Variscan mountains (Geluk, 2005). When the thermal anomaly associated with this Variscan orogeny started to decay (i.e. the lithosphere cooled down), regional thermal subsidence occurred starting from the Permian (De Jager, 2007). The Netherlands area was characterized by a typical dry climate from the Permian until the Late Triassic, which was due to its geographical position in the arid climate zone as well as being on the leeward side of the Variscan mountain range (Geluk, 2005).

2.1.2 Permian

This was the onset of the Southern Permian Basin which started to fill up with the Rotliegend sediments from the surrounding mountain ranges: in the south the basin was bordered by the Rhenish Massif and London-Brabant Massif, to the north by the Mid North Sea High and Ringkøbing-Fyn High (Geluk, 2000). The geographical location of this basin was in the arid climate zone at approximately 10 to 20 degrees North, comparable to the latitude of the modern-day Sahara desert. Moreover, the Variscan mountains in the south shielded the basin from humid trade winds from the Tethys Ocean, which also contributed to the dry environment (Glennie, 1998). The extension associated with lithospheric cooling provided the accommodation space and the Variscan mountains provided large amounts of sediment input which allowed the basin to remain a large depocenter. From south to north, the stratigraphic sequence of the Rotliegend comprises conglomerates, aeolian sandstones, fluvial sandstones, lacustrine silts, claystones and in the upper north intercalations of evaporites. Given that Noord-Brabant is located just north of the London Brabant Massif, the main depositional environments were the alluvial fans from the Variscan Mountains and large aeolian sand dunes. This extremely arid climate was maintained as the basin continued to deepen, which caused saltwater influx from the nearby sea to catastrophically flood the basin and deposit evaporites. By the late Permian, a salt package of locally more than 1500 m in the axial zone of the Southern Permian Basin had formed. This formation topped the underlying Rotliegend clastics and is known as the Zechstein salt (De Jager, 2007).

2.1.3 Triassic

The Triassic basin development occurred during ongoing thermal subsidence as a result of the continental break-up of supercontinent Pangea. It wasn't until the Early Cretaceous that the rifting had mostly ceased in the Netherlands area, which had drifted northwards and was at that time located in the sub-tropical climate zone

(fig. 1). The Lower Triassic Lower Buntsandstein consists of fine-grained clastics (i.e. mudstones) which were deposited in brackish to saline lacustrine environments also known as playa lakes (Winstanley, 1993). Here a playa lake is referred to as a flooded salt flat in an intracontinental basin (Briere, 2000).

The overlying Main Buntsandstein contains a cyclic sequence of coarser fluvial and aeolian clastics and consists of three main formations: Volpriehausen, Detfurth and Hardegsen (De Jager, 2007). The Roer Valley Graben was the sediment sink for the alluvial fan systems originating from both the London Brabant Massif and the Rhenish Massif. Base level changes and phases of fault reactivations were the cause for four episodes with large alluvial fan deposits: Volpriehausen, Detfurth, Hardegsen and Röt (Winstanley, 1993). The deposition of evaporites, with their characteristic high sedimentation rate and relative high mass, increased the differential loading of the basin and deepened the grabens even further (Geluk, 2005).

The Middle Triassic was marked by an increased marine influence due to a first connection with the Tethys Sea, which is reflected stratigraphically by a sequence of claystones and carbonates. Furthermore, discontinuous connections with the sea led to the deposition of evaporites in marginal sabkha environments (Geluk et al., 2005, Winstanley, 1993). Important formations of the Middle Triassic are the Solling, Röt (mainly lagoon deposits) and Muschelkalk (carbonates and dolomites), as well as Lower and Middle Keuper (De Jager, 2007).

The Late Triassic was marked by slow but continuous regional subsidence. Due to the paleogeographic position at 40 degrees N and the erosion of the Variscan mountain range, the climate became more humid (McKie, 2017). By the Early Jurassic, the formation of a wide epicontinental sea allowed for the deposition of up to 1800 m fine-grained clastic sediments of the Altena Group (De Jager, 2007).

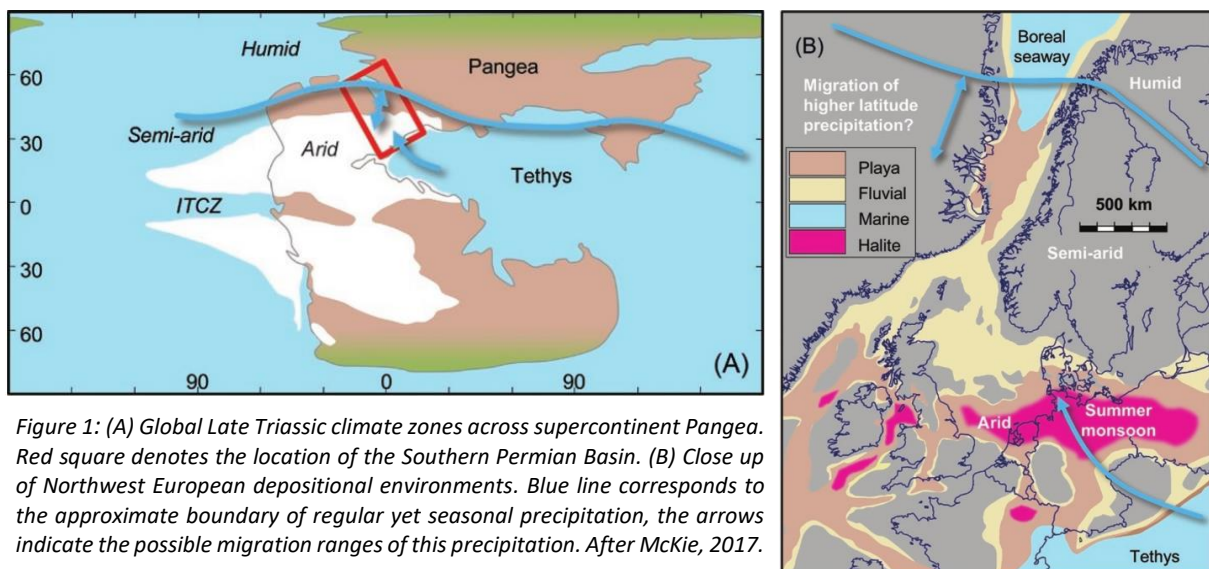


Figure 1: (A) Global Late Triassic climate zones across supercontinent Pangea. Red square denotes the location of the Southern Permian Basin. (B) Close up of Northwest European depositional environments. Blue line corresponds to the approximate boundary of regular yet seasonal precipitation, the arrows indicate the possible migration ranges of this precipitation. After McKie, 2017.

2.2 Tectonic evolution

Even though both the Permian and Triassic basins were common sediment sinks, the tectonic mechanism behind their formation is rather opposing. The Permian basin formed during the late stage of Pangea's assembly in a compressional regime, by the process of late orogenic extension (Van Wees et al., 2000). The phenomenon of extensional basin formation with ongoing mountain building has been linked to lithospheric root removal or slab detachment (Vissers, 2012). The consecutive breakup of Pangea was accompanied by large-scale rifting and resulted in the formation of the Triassic basin, which thus originated from an extensional regime. At that time the thin-skinned and thick-skinned tectonics displayed the same extensional features in the Southern Permian Basin, although apparently without igneous activity (De Jager, 2007).

The Carboniferous tectonic setting largely dictated the development of the basement and continued to influence the overlying formations throughout their evolution. The sediments that would evolve into the main hydrocarbon reservoirs were deposited during the Middle to Upper Permian (Rotliegend) and Triassic (Main Buntsandstein) in their typical dry climate. It was not until the Late Triassic that the Netherlands experienced

more periodically humid environments, which can be contributed to the higher latitude and erosion of the Variscan mountains, which could no longer shield the basin from humid air masses flowing northwards (Geluk, 2005).

2.3 Structural elements & stratigraphy

Fluctuations in the lithospheric stress regime have controlled the passive rifting of the Roer Valley Graben. Even at present day, intraplate stress with NW-SE orientations still contribute to seismic activity such as the earthquake in Roermond (M=5,4) in 1992 (Geluk et al., 1994). The passive rifting of the Roer Valley Graben is accompanied by the rise of the Moho discontinuity by 2-3 km, whereby this boundary currently lies at 28 km depth below the graben axis (Zijerveld et al., 1992). As a consequence, the pre-existing structural framework inherited from the Permo-Carboniferous influenced the development of the graben. The Roer Valley Graben has been a major depocenter for the surrounding mountain ranges. The London Brabant Massif in the southwest and the Rhenish Massif in the east would fill up the subsiding basin with up to 2000 m of Cenozoic sediments (Geluk et al., 1994)

The RVG is surrounded by structural highs or platforms, except for the West Netherlands Basin in the northwest (fig. 2). The boundary between the RVG and the WNB is defined as the pinch-out of Upper Cretaceous sediments, where the Chalk Group has been eroded as a result of strong inversion in the WNB (Kombrink et al., 2012). For the West Netherlands Basin, paleo-environments have been linked to present-day porosities (Ursem, 2018). Figure 2 shows the occurrence of all Triassic intervals in all wells in the southern Netherlands. The low density of Triassic intervals within wells in the Roer Valley Graben is obvious.

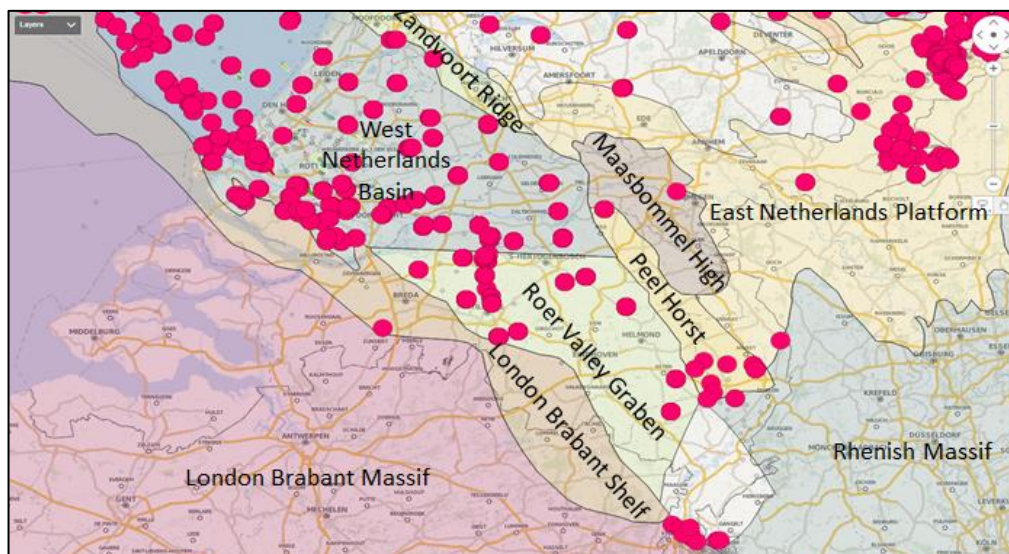


Figure 2: Structural elements overlying topography. Pink dots denote all the well locations that contain Triassic intervals.

The Triassic stratigraphic interval in the Netherlands is sandwiched between the Permian Zechstein and the Jurassic Altona Formation (fig. 3). The Triassic is composed of the Lower Germanic Trias Group (RB) and the Upper Germanic Trias Group (RN). The Lower Germanic Trias Group contains the members: Lower Buntsandstein, Volpriehausen, Detfurth and Hardegsen. The Upper Germanic Trias Group contains the members: Solling, Röt, Muschelkalk and Keuper (Geluk, 2007).

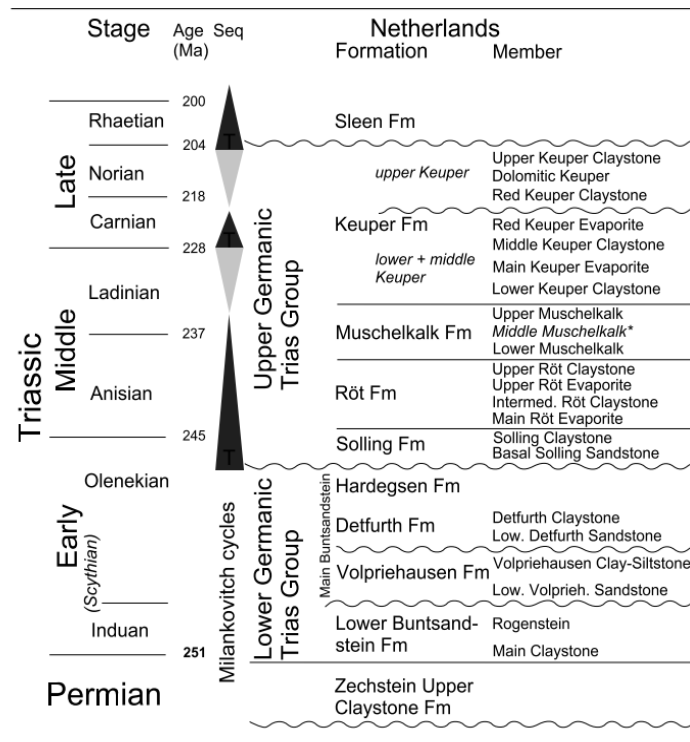


Figure 3: Lithostratigraphic subdivision of the Triassic in the Netherlands. After Geluk, 2007.

3. Petrophysical background

Generally, a volume of reservoir rock is composed of a matrix with a certain amount of porosity ϕ , which may be filled with water, oil or gas. These phases all show a distinct fluid density. The matrix (or the grains) also has its own density, i.e. the matrix density or grain density. The weighted average of the fluid density and the grain density yields the bulk density. The bulk density can be measured via the wireline and is known as RHOB. For grain density measurements core plugs must be taken. Porosity is given as a volume fraction or percentage (fig. 4) and gives a first rough impression of hydrocarbon or geothermal storage potential. However, for actual production of the reservoir, the ability for flow through the pores is important.

The effective permeability k consists of the intrinsic permeability and the relative permeability. The intrinsic or absolute permeability depends on the pore diameter and pore connectivity, which together describe the pore structure. This is a measure of the compaction and therefore dependent on the porosity. Relative permeability comes into play in multi-phase Darcy flow, e.g. in a mixture of oil and water. The effective permeability is the intrinsic permeability times the relative permeability (Hantschel & Kauerauf, 2009). The transmissivity of a layer is the product of the arithmetically averaged horizontal permeability (mD) and the layer thickness (m), hence has the unit Darcy meter (Buik et al, 2016).

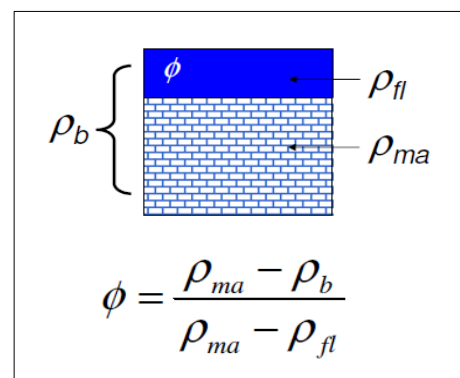


Figure 4: Visualization of a porous medium and related porosity calculation.

The reservoir quality largely depends on three major consecutive components: facies, maximum burial and diagenesis. The first and foremost control is facies, when sediments are deposited with their specific grain size, shape and sorting, therefore immediately affecting porosity. When the sediments are buried deeper, mechanical compaction decreases the porosity from the original facies. Upon more burial, higher temperatures allow the

chemical processes of diagenesis, which may result in both pore enhancement and reduction. Therefore the present-day porosity may be the sum of all three processes. A brief overview of these three reservoir quality controls will be given here.

3.1 Facies

Typically, an increasing porosity goes hand in hand with an increasing permeability. This poro-perm relation is due to the sorting and size of the grains (Sneider, 1987). Since the sorting and grainsize are in the first place determined by the depositional setting and hence facies, poro-perm plots can provide a better distinction of the facies (Slatt, 2013). When discussing facies and classification the terminology can be slightly confusing, so the definitions from figure 5 are used.

Facies	A body of sedimentary rock with specific color, bedding, composition, texture, fossils and sedimentary structures.
Lithofacies	The set of compositional and textural characteristics that permits the sediment to be distinguished from others.
Electrofacies	The set of log responses that characterizes a sediment and permits the sediment to be distinguished from others.

Figure 5: Definitions after Geel & Lutgert, 1990.

A classification has been made based on depositional environment, rather than the typical lithofacies classification with facies codes (Miall, 1985), as there are a number of lithofacies groups with some overlap. The main facies that are recognized in the current wells are stacked sheetfloods or floodplains with minor channeling, (ephemeral) floodplain ponds or lakes, fluvial channels, braided channel complexes and overbanks. Floodplains are characterized by a relatively low-energy depositional environment (Ursem, 2018). Facies interpretations for alluvial fans and fan deltas are not incorporated in the studied wells, since they are not described in the lithology logs. The use of facies classification allows for the creation of poroperm trends per lithology, as shown in figure 6.

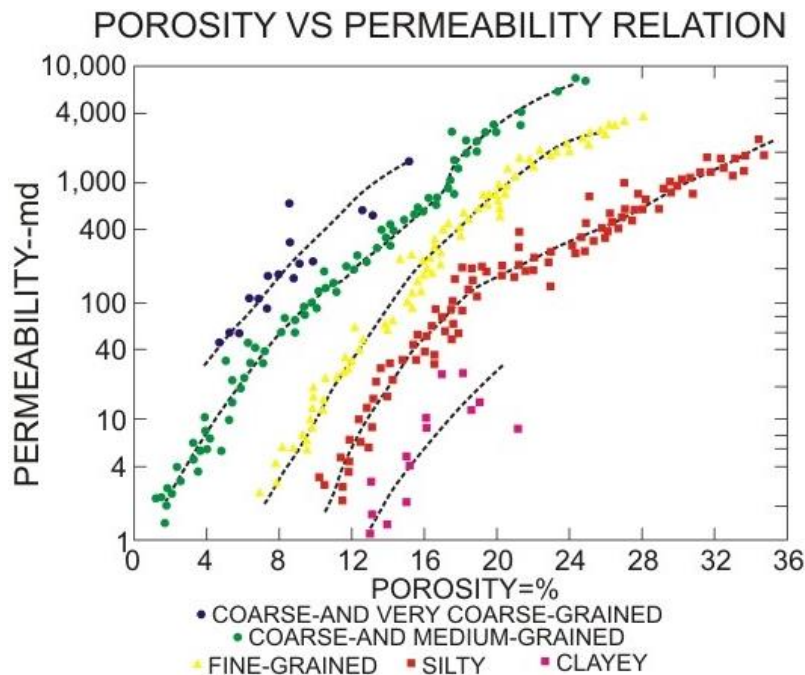


Figure 6: Poro-perm trends per lithology. Sneider, 1987.

3.2 Burial

Athy's Law (Athy, 1930) describes the exponential decrease of porosity with depth: it states that rock becomes more compacted the deeper it is buried. The maximum burial (MB) is the largest depth at which the rock has been buried, and following Athy's Law, MB is therefore a measure of the expected porosity. Hiatuses in the overlying sedimentary record interpreted as eroded strata and inversion structures may indicate that the maximum burial depth differs from the present-day depth. The burial anomaly (BA) describes the difference between the current depth and the maximum burial depth. The maximum burial temperature can be determined from a geothermometer such as vitrinite reflectance (VR). Since vitrinite forms diagenetically from plant material (e.g. cellulose), the highest reflectance may be found in terrigenous shales and marls, and the least in clean sands, carbonates and evaporites (Barker et al., 1986).

3.3 Diagenesis

Diagenesis is a process that can both decrease and increase the reservoir properties. The two most important chemical mineral reactions that decrease the porosity during burial are quartz cementation and shale diagenesis. The poro-perm relation seemingly does not hold above approximately 120 °C as the permeability decreases exponentially. Below 3000 m depth, illite minerals start to form from smectite clay. The effect of illite formation is minor with respect to the porosity, but it has a large impact on the permeability. Illite precipitates as micropores, which requires a small amount of diagenetic clay to create a very large permeability reduction (Bjørkum & Nadeau, 1998; Pallatt, Wilson & McHardy, 1984).

Illite, kaolinite and grain leaching are related by the process of fibrous illite nucleation in sandstones. The reaction occurs above 150 °C and is: Kaolinite + K-feldspar → Illite. Kaolinite is a primary reactant and potassium is derived from in-situ K-feldspar grain dissolution or imported into the model reference frame. This leads to the formation of fibrous illite and secondary porosity in sandstones (Lander & Bonnell, 2010).

4. Methods

The general hypothesis for the Roer Valley Graben is that there is a strong link between facies, or provenance, and maximum burial depth. The idea behind this concept is that the flanks of the structural highs surrounding the RVG are more proximal with coarser sediment, whereas the deepest center has been the depocenter for the distal, fine-grained sediment. A similar trend has been identified in the Middle to Upper Jurassic of the northeastern North Sea (Ramm, 2000). This relationship is not as clearly present in the adjacent West Netherlands basin (Vis et al., 2010), whereas the Roer Valley Graben appears to be a much more 'intact' basin with less tectonic reactivation affecting the burial depth of the reservoir. Due to this strong relation between facies and maximum burial, the electrofacies approach might prove a useful method. Electrofacies modelling is explored in this study by means of cluster analysis and finally lithology prediction.

4.1 Data handling / selection

First an overview of the available data must be made. Data from the following studies/datasets has been included: NLOG, NuTech, Clyde, BP and NAM. The Nederlands Olie- en Gasportaal (NLOG) is the public database of Dutch subsurface data. Log interpretation has been done with the help of Petrel. The results of property tests on core plugs have been analyzed with Spotfire. The locations of the wells that have been used for electrofacies modelling are shown in figure 7.

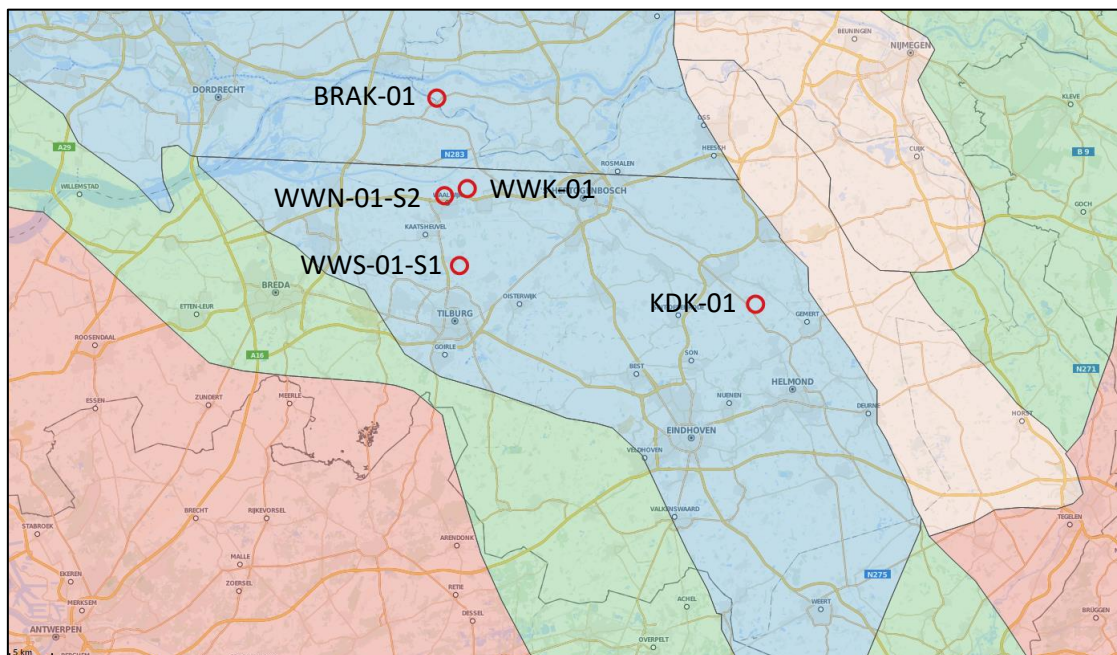


Figure 7: Location of wells. Geographical distribution of the wells and the main structural elements. Blue = deep basin; red = main structural high; lighter red = minor high; green = platform.

4.2 Log interpretation

The distinct log responses from different facies are covered by the term electrofacies (Serra, 1983). Some of the most common logging techniques that are used for down-hole measurements are briefly discussed below. These in situ techniques provide information on the lithology, porosity, water saturation and occurrence of hydrocarbons. However, down-hole permeability can only be determined indirectly from measurements on core plugs in the laboratory. The porosities derived from these in permeabilities are then matched to the logged (i.e. down-hole) porosities to estimate permeabilities along the entire drilled section.

Table 1: Wireline logs and their respective properties.

Log	Log type	Unit	Measures	Use	Pitfall
GR	Gamma ray	API	Natural gamma radiation from decaying U, Th and K	Sand/shale differentiation	Mica-effect in sands resembles shale response
RHOB	Bulk density	g/cm ³	Electron density	Cementation trends	Porosity and cementation affect bulk density
NPHI	Neutron porosity	%	Returned neutron count from H and Cl interaction	Porosity	Clay resembles fluid response
DT	Sonic / Acoustic	us/ft	Travel time through formation / slowness / inverse of velocity	Tight/porous differentiation	Fractures disturb sonic response
RT	Resistivity	Ohm*m	Resistive properties of fluid/gas	Water/gas differentiation	Oil-based or water-based mud required
CALI	Caliper	inch	Borehole diameter	Changes in size and shape of borehole	Less useful for geological interpretation

A well template for proper evaluation and comparison has been designed. The well template comprises both raw data and derived values. The included wireline logs are the gamma ray, sonic, caliper, bulk density (RHOB), neutron porosity (NPHI), water saturation and resistivity log. The core plug measurements include the porosity, horizontal permeability, vertical permeability, grain density. Note that the measurements of the wireline logs are determined in situ, whereas the core plug measurements are determined at surface. Derived values include the porosity from the bulk density (PHI-RHOB), porosity from the neutron porosity (PHI-NPHI) and the average calculated porosity (PHI-RMS). The latter is the average of the neutron porosity and the bulk density porosity by means of the root mean square to correct for any present gas. The presence of gas would cause the bulk density porosity to appear higher and the neutron porosity to appear lower (Benedictus et al., 2007).

4.3 Electrofacies modelling

For the following part of this study, it is important to repeat the definition of electrofacies: an interval in a borehole with a distinct log response. These log responses may then be recognized in other intervals in the same well or in other wells and linked to facies. The input for lithology predictions is thus the relation between the established lithofacies from a small number of intervals and the corresponding log responses. There are numerous techniques available, of which two are tested here. Ultimately, these techniques aim to unravel and to bring structure to the data.

When a cloud of data points requires structure, it can be divided into groups. Clustering means the division of objects into groups (clusters). When assigning particular labels to these groups, it is called classification. For classification, the labels that are given to data groups must be discrete values. There are also prediction models with continuous attributes, which is regression. The classification model can then be used both as a descriptive or a predictive tool. With a predictive model, the aim is to predict the classification label of an unknown data point (Kumar et al., 2005). For this study, that would be to predict the lithofacies of a data point in the space of e.g. the gamma ray, RHOB and resistivity logs.

To get acquainted with the concepts of clustering and electrofacies, the first electrofacies analysis was performed with a program that uses K-means clustering: Wkmeans. Although Wkmeans is able to make classifications, it is not able to use the lithofacies from core analyses as input. Since this discrete lithofacies classification is required to check the validity of the prediction, a different method has been searched for and found in Petrel. The workflow for both programs is given below.

4.3.1 Cluster analysis in Wkmeans

Cluster analysis is used to show the probability that a log interval belongs to a certain facies group. This helps in assigning potential facies to the intervals.

In short, cluster analysis can be defined as the division of data into meaningful or useful groups (Kumar et al., 2005). The grouping is based entirely on information found within the data. The aim is to create groups with small differences between the objects within the groups, and large differences with other groups.

There are numerous specific clustering techniques available, e.g. agglomerative hierarchical clustering, DBSCAN and K-means, with the latter being one of the most commonly used clustering techniques (Kumar et al., 2005). Given the know-how and availability of the software that uses K-means clustering, this clustering technique has been explored with Wkmeans.

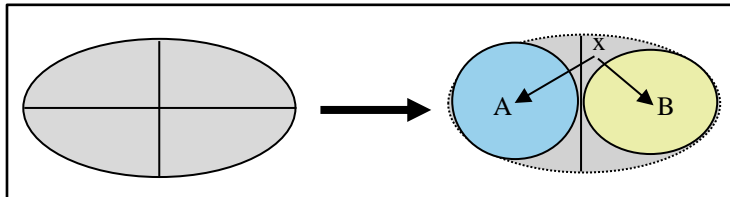


Figure 8: Schematic overview of k-means clustering. Division of a cluster yields two new centroids (A and B) and re-assignment of data point x.

K-means clustering attempts to find a fixed number of clusters (k) from the data points. The clusters are defined by their centroid, usually the mean of the points. These centroids or cluster centers are calculated as follows. First, it is assumed that all data points belong to the same group (fig. 8). Next, the group is divided through the middle of the variable with the largest variance, creating two groups. The data points are then assigned to the group with the nearest centroid, causing this group center to slightly shift again. The re-assignment of the points stops when the cluster centers have become stationary. Finally, there will be two new clusters with centroids and new distances to the individual data points (Kumar et al., 2005). Hence, $k = 2$ in this case. These clusters can be split into more clusters and the re-assignment process will be repeated. For facies intervals, a maximum of 10 groups is usually sufficient.

The program Wkmeans uses the k-means clustering algorithm as it was developed by Hartigan, 1975, which uses the mean of a set of data points from logs to assign them into clusters. Since logging tools are calibrated differently, normalized log responses must be taken for proper comparison. The cluster analysis has been performed on intervals of three wells within the area: KDK-01, WWK-01 and WWS-01-S1. For each interval, an extensive geological report is available in the literature with core descriptions, plug data, lithofacies descriptions and interpretations of the depositional environment.

Besides displaying the colored clusters in 2D and 3D space, Wkmeans shows the intervals in the well that correspond to each cluster. Moreover, a graph with the PFS is visualized. The PFS or Pseudo-F statistic is the statistical optimum with the best fit or the ideal number of clusters (Vogel & Wong, 1979). The PFS is also referred to as the 'goodness' of the clustering (Kumar et al., 2005). This means that the data points in a multi-dimensional cloud can be clustered with the least scattering, i.e. the division into different groups or clusters is the most ideal and the interstitial differences within the clusters are the smallest. Often a cluster tool will provide an optimum at only 2 clusters, generally related to an obvious sand/shale lithofacies distinction. It is up to the geologist to select a more meaningful number of clusters based on log and core responses.

4.3.2 Lithology prediction in Petrel

It is possible to extend this workflow by using a neural net: each time the algorithm assigns a facies, the output can be corrected with the given input facies. The neural net then learns what the preferred output must be, and will hopefully give an enhanced result. This will be explained below in more detail.

With the Quantitative Analysis tool in the Advanced Geophysics perspective in Petrel, it is possible to assign a particular lithofacies to a distinct interval of log responses. This advanced tool uses probabilistic prediction and artificial intelligence through a neural net. Core descriptions and facies interpretations from literature have been

used as input for the modelling, whereby the facies have been manually added to the intervals in the well sections.

We have seen that Wkmeans only allows an unsupervised classification whereby the input data is subdivided into classes. In order to make predictions that may be verified by our own input, a supervised classification is required. Supervised classification is possible in Petrel via the 'Quantitative Interpretation' tab in the Advanced Geophysics perspective. The schematic workflow for the litho-classification and prediction tools is shown in figure 9.

The lithology prediction has been performed on intervals of three wells within the area: BRAK-01, KDK-01 and WWN-01-S2. Note that again no seismics is used in this analysis.

Prior to lithology prediction, QC of the logs may show the need for a core shift to fit the plug measurements with the wireline data.

The first step of lithology prediction is defining the input. We manually mark the discrete log with the facies interpretation from the lithological logs (Appendix II). Here a number of different Litho classes (i.e. facies) must be defined and given a distinct color. This facies log represents the training set and is then used as one of the input parameters in the litho analysis, together with the global well logs, the wells and top and base markers. A prior probability can be set for the different Litho classes. Furthermore, it is possible to assign the number of bins, the upscaling factor and the inversion error factor to the selected global well logs. QC of the defined input will show the PDF confusion matrix and potential errors and warning messages. The result of the Litho analysis is the Probability Density Functions curve, which can be visualized in 2D and 3D, and which represents the variability in formation properties given by the wells. The PDFs are part of the model that makes the predictions.

Next is the lithology prediction, which has been performed by two different learning algorithms. The standard learning algorithm in Petrel is the Bayes classifier. Bayesian statistics use empirical observations to recalculate the probabilities of an event, in this case of a certain facies belonging to a certain log response. In practice, the Bayesian approach means that uncertainties of the logs can be incorporated (Hantschel & Kauerauf, 2009). Here the input is given by the previously defined Litho Analysis, the input type (here: well logs), the wells, the attributes (here: global well logs) and the zone of interest with the top and base markers. The output can be visualized as a discrete log in the well section. Note that this lithology prediction is based on the probability density functions, i.e. on the probabilities of occurring as a particular facies.

Besides the standard lithology prediction workflow with PDFs, there is another classification technique available. The neural network distinguishes itself from other classifiers by a few aspects. First of all, the modelled output is compared to the target (i.e. equal to the input) data to determine an error. The errors are then back-propagated through the network and the different weights of the data are adjusted, creating a smaller error. Moreover, this workflow is iterated until it has reached the best possible fit.

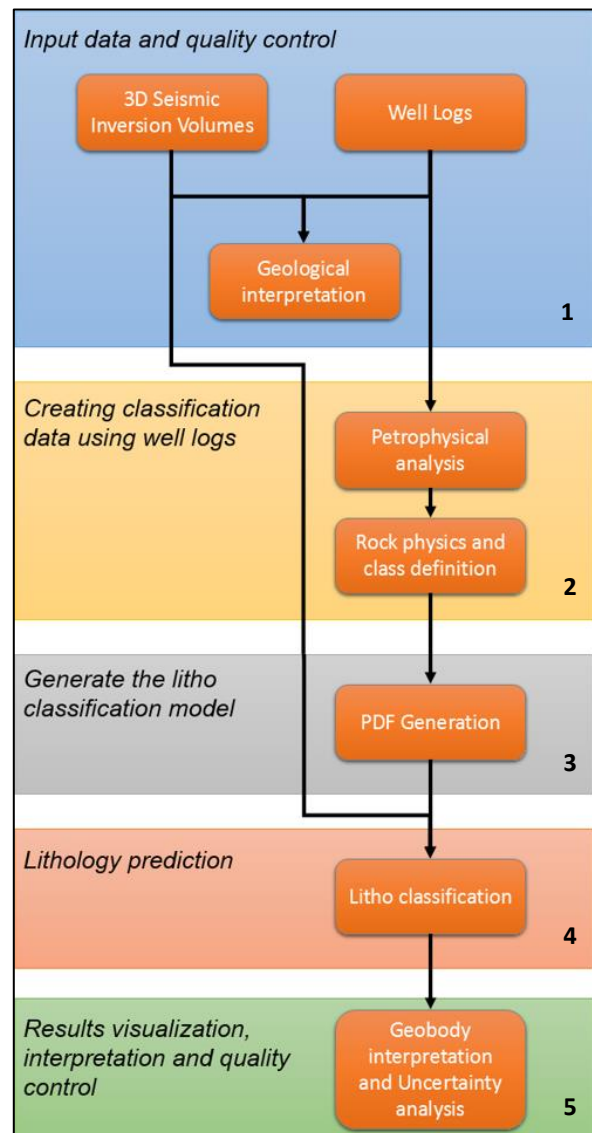


Figure 9: Workflow as performed in Petrel.

The neural network in Petrel allows for both supervised and unsupervised learning. The supervised learning compares the outcome of the calculations with the correct results that were given by us, which is how it can learn (Hantschel & Kauerauf, 2009). Therefore the input for the neural net prediction are the wells and the global well logs, and the neural net is supervised by the manual litho classification. Since the neural net requires training, the following settings have to be selected: the maximum number of iterations, the error limit (%), the cross validation (%) and the probability threshold. Additionally the facies classification of the input log must be selected as the supervising Neural net class, i.e. the predictions will use the supervised classes that we manually assigned to the logs. The output can again be visualized as a discrete log in the well section.

Table 2 shows the available cored intervals that have been used as input for the classification. As it becomes clear that only a handful of the Triassic intervals has been available for core studies, the need for more facies interpretation is emphasized.

Table 2: Wells and related members that have been used as input for the classification.

Well code	BRAK-01	WWK-01	WWN-01-S2	WWS-01-S1	KDK-01
Well name	Brakel	Waalwijk	Waalwijk Noord	Waalwijk Zuid	Keldonk
Upper core members	RNROF	RNROF, RNROY	-	RNROY	RNROF, RNROY
Lower core members	RBMD C	-	RBMVL, RBMVU, RBMVA, RBM D U, RBMH	-	RBMVL
QC	Good	Low resolution of input litholog	Good	Interval of only 6,5 m	Good

5. Results

First the influence of the three main controls on reservoir quality is briefly discussed, as well as the problems that occur with the current methods. Next the results of the electrofacies modelling are shown, both for the unsupervised and supervised facies classification.

5.1 Controls on Reservoir Quality

The quality of a hydrocarbon or hydrothermal reservoir is controlled by three main consecutive factors: facies, mechanical compaction and diagenesis. A concise overview of the influence of these controls on the Roer Valley Graben is given below.

5.1.1 Facies

Often the porosity ranges within an interval are due to the ranges that exist within a facies. A channel sequence shows a fining upwards sequence and thus a larger range of grain size and porosity (Serra, 1983). This trend is reflected by the wide range in porosity measurements on porosity-depth plots.

A depositional model for East Brabant during the Triassic based on previous models from Leeder & Gawthorpe, 1987 and Ursem, 2018 is shown in figure 10. It shows the location of the Roer Valley Graben between the mountain ranges of the London Brabant Massif and the Rhenish Massif. The insets show a close-up of the local depositional environments.

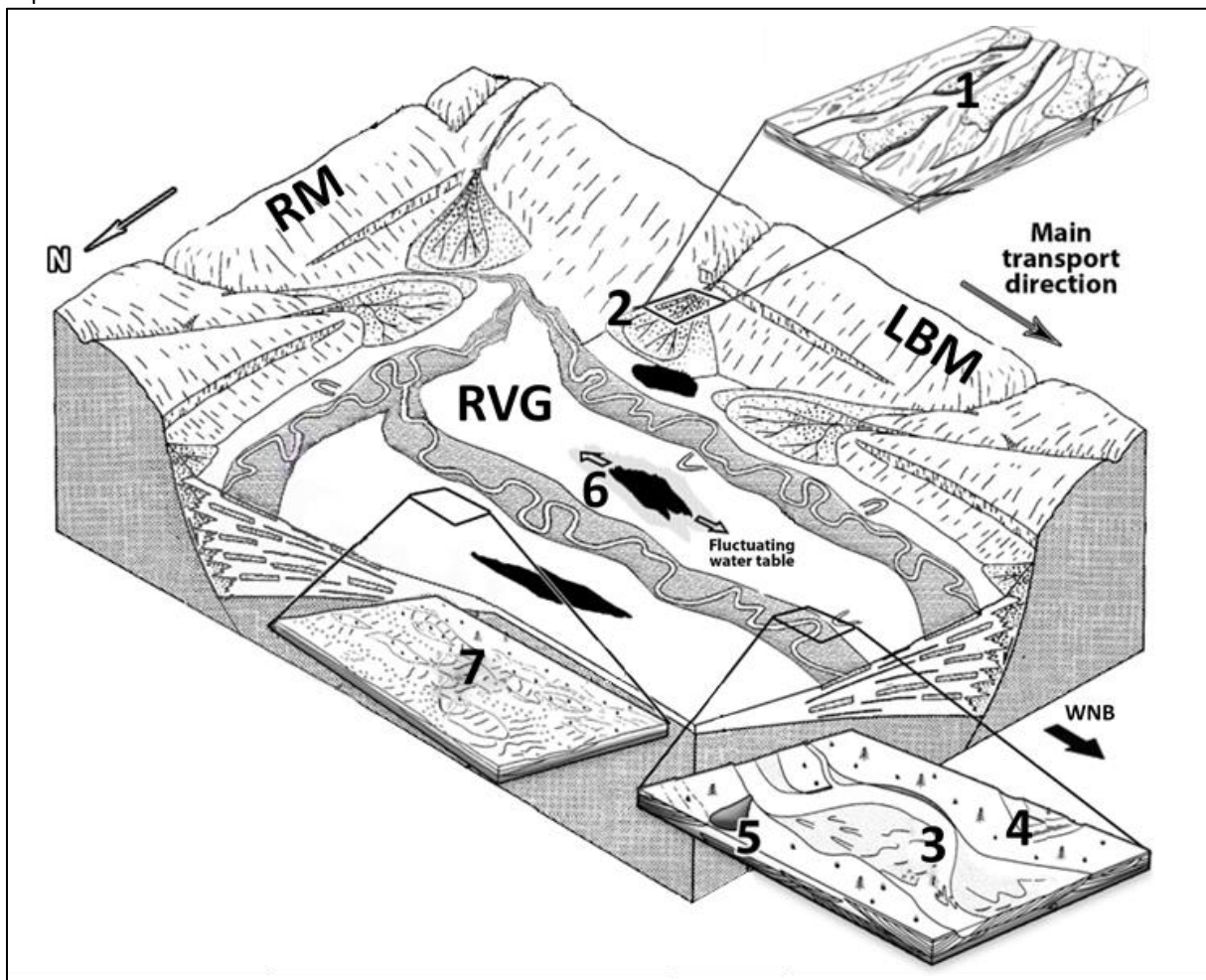


Figure 10: Depositional model for the Roer Valley Graben during the Triassic. RM: Rhenish Massif, LBM: London Brabant Massif, RVG: Roer Valley Graben, WNB: West Netherlands Basin. Facies types: (1) alluvial fan, (2) fan delta, (3) braided river channel, (4) abandoned channel, (5) mudflow, (6) (ephemeral) pond/lake, (7) floodplain with minor channeling. After Leeder & Gawthorpe, 1987 and Ursem, 2018.

5.1.2 Burial

Burial history plots of several wells within the Roer Valley Graben showed that the maximum burial depth often corresponds with the current depth of the formations in Brabant. A minor burial anomaly in the southwest of the graben can be ascribed to the late-stage tectonic reactivation starting from the Pliocene (4 Ma), which led to an uplift of locally 150 m (i.e. NDW-01). Based on basin modelling studies (Nelskamp & Verweij, 2012), it is assumed that a burial anomaly of less than 300 m has no significant effect on the physical properties of the rocks. Major fluctuations within the porosity range are therefore not expected from burial anomalies, but from other elements constraining the reservoir quality such as facies and diagenetic processes. From these observations it can be concluded that the present day burial depth is equal or close to the maximum burial depth and hence, no additional corrections are required.

5.1.3 Diagenesis

To determine the influence of diagenesis on porosity, the following analysis has been performed. The depth-porosity plots in figure 11 have been constructed for the well with the largest number of plug measurements, WWN-01-S2. The data points have been grouped in discrete bins, applying the same method as Van Kempen et al., 2018. The depth-porosity plot of core plugs from well WWN-01-S2 shows a wide range of grain densities, without the typical depth-trend. This most likely indicates that diagenesis has affected the porosity locally. With depth, porosity decreased due to mechanical compaction, whereas the matrix density (i.e. grain density) does not change merely due to mechanical compaction. This means that the grain density must have been affected by diagenetic processes. Dolomitization has been found in cores and is visible on core photos (NLOG).

A discrepancy in measurements and trends from this interval indicates that it probably is not possible to compare this trend to plug data from other wells, members and intervals. In other words, these trends cannot be used for the larger scale. The wells from the RVG that are used in this plot are: AST-01, BKZ-01, DON-01, HSW-01, HSW-01-S1, KDK-01, LOZ-01, OIW-01, SPC-01, SPG-01-S2, VEH-01, WAP-01, WWK-01, WWN-01-S2, WWS-01-S1.

The distinction of grain densities within a porosity-depth plot has been successfully applied for the RBMVL (Van Kempen et al., 2018). Even when using different stratigraphic intervals (i.e. all available Triassic intervals), a similar trend appears to emerge from our much smaller dataset.

At a local scale, the combination of facies, depth and diagenesis makes the comparison of intervals rather complicated. Therefore a lithology prediction based on log responses is explored.

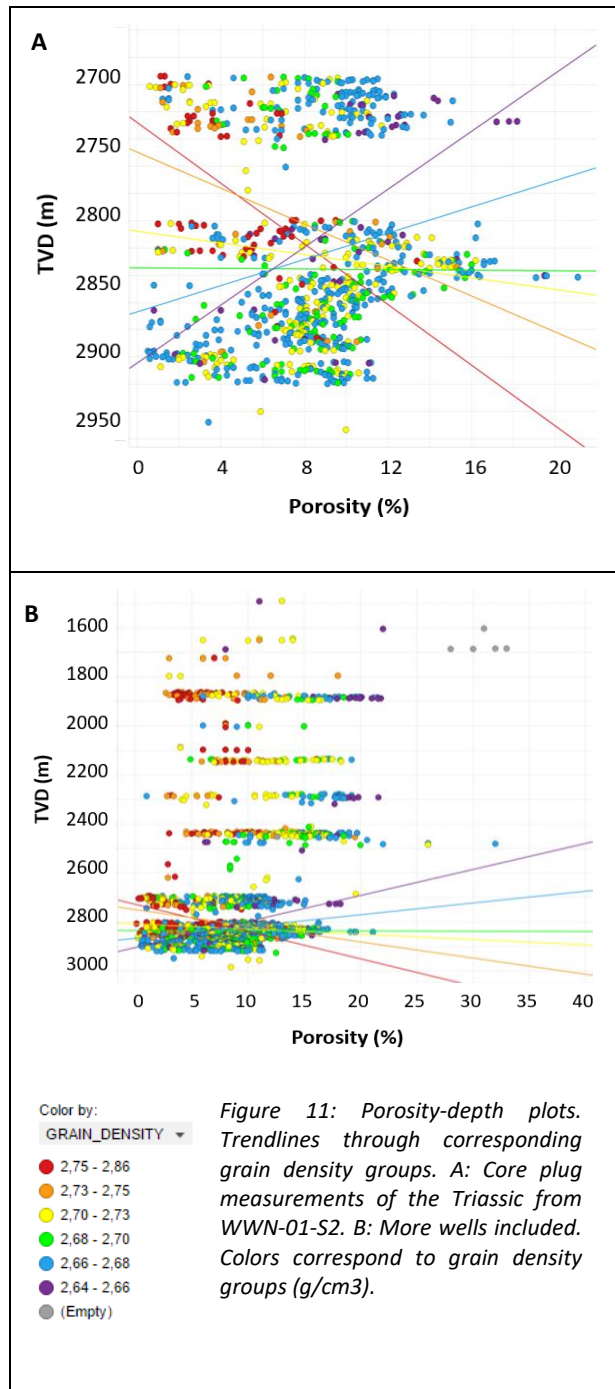


Figure 11: Porosity-depth plots. Trendlines through corresponding grain density groups. A: Core plug measurements of the Triassic from WWN-01-S2. B: More wells included. Colors correspond to grain density groups (g/cm³).

5.2 Cluster analysis in Wkmeans

The results of the k-means clustering are discussed per well interval. Intervals of good and poor correlation will be shown.

Cluster analysis has been performed on the cored intervals of wells BRAK-01, KDK-01, WWK-01 and WWS-01-S1. For well WWN-01-S2, the interval comprises the member sequence of RBMVL, RBMVU, RBMVA, RBMDU and RBMH. However, the input consists of only two wireline logs, i.e. the gamma ray and sonic log. Furthermore there is no suitable data table available to load in Wkmeans, so for this well no cluster analysis has been done.

5.2.1 BRAK-01

Two intervals with available lithologs have been analyzed. The upper interval lies within the RNROF, the Röt Fringe Sandstone Member, the lower interval lies within the RBMDC, the Detfurth Claystone Member.

Upper interval (fig. 12)

The upper interval of 20 m is measured from 2349 – 2369,10 mBRT. The main depositional settings were (1) fluvial channel, (2) floodplain pond/lake, (3) floodplain pond/lake with influence of sheetfloods, (4) sheetfloods with minor channeling/scouring and (5) sheetflood.

Input logs for the cluster analysis are gamma ray (GRC), bulk density (RHOBEDIT) and resistivity (RT). A core shift of 1,5 meter upwards yields a better match with permeability measurements from plugs. This shift is also used to change the input interval of the cluster analysis. When compared to the interpreted depositional environments, there appears to be a better match between changes in log responses and facies boundaries.

The statistical best fit is taken at 5 clusters. Here the floodplain pond/lake and floodplain pond/lake with influence of sheetfloods are well distinguished from the clustering. As a lithofacies that is influenced by different environments with a wide range of log responses, the sheetfloods with channeling are not recognized as one cluster. The channel cluster can be recognized in the 'mixed' lithofacies of sheetfloods with minor channeling.

Lower interval (fig. 13)

The lower interval of BRAK-01 is measured from 2452 to 2478,65 mBRT. A total number of 12 individual environments are interpreted from the sedimentary analysis, which have been grouped here into 3 main depositional settings: (1) floodplain pond/lake, (2) sheetfloods and (3) braided channels. Many of the interpreted environments have mixed deposits in a transitional zone.

Input logs are the gamma ray (GRC), bulk density (RHOBEDIT) and resistivity (RT). A core shift of approximately 2 m upwards gives a better match with permeability measurements and facies interpretations. The core shift has been adopted in the cluster analysis to compare the same intervals.

The PFS plot shows that the best fit is found for 3 clusters. The best match between lithofacies and clusters is from the floodplain ponds, with all 6 interpreted pond intervals represented by the clustering. The sheetfloods and braided channels are more difficult to distinguish from the cluster analysis. The lowest stacked sheetfloods interval stands out from the others according to the cluster analysis, and this is supported by high permeability measurements.

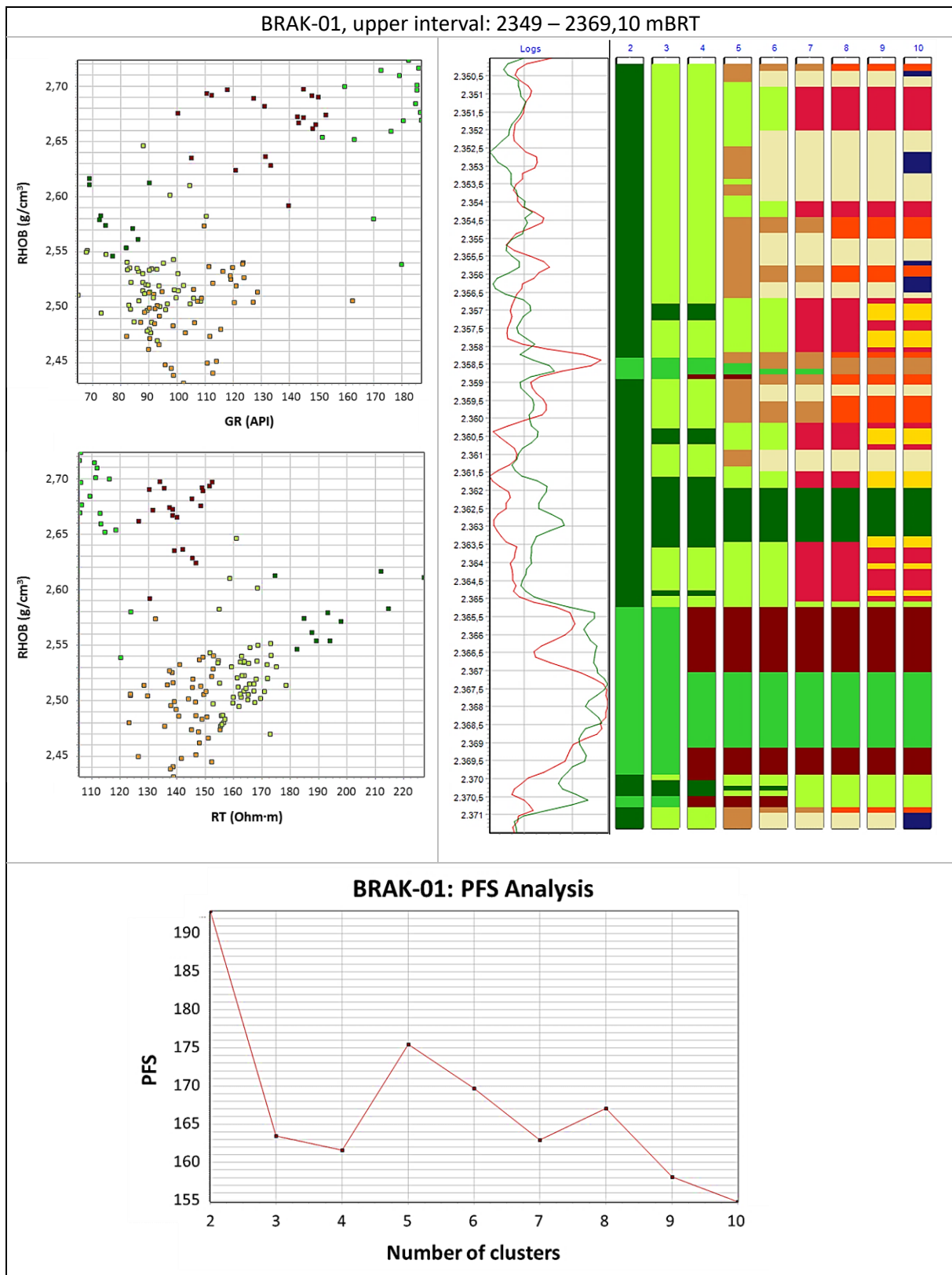


Figure 12: Results of Wkmeans modelling for the upper interval of BRAK-01. (A) and (B): wireline data with their corresponding cluster. The number of clusters (i.e. 5) corresponds to the optimum derived from the PFS plot. (C): Distribution of clusters along the borehole interval. Each column represents the number of clusters, starting from 2. (D): PFS plot with the optimum number of clusters.

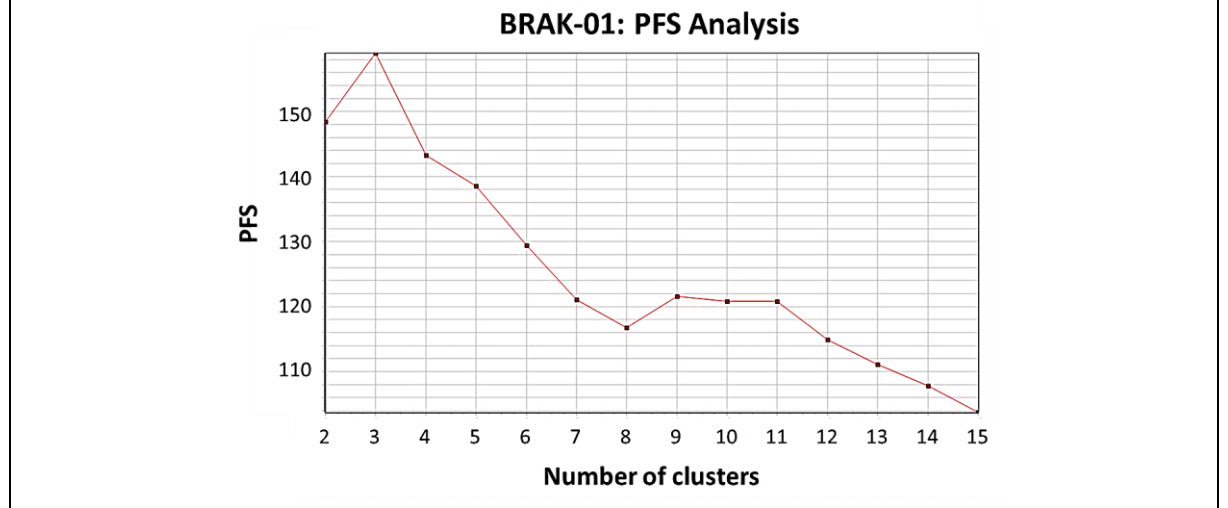
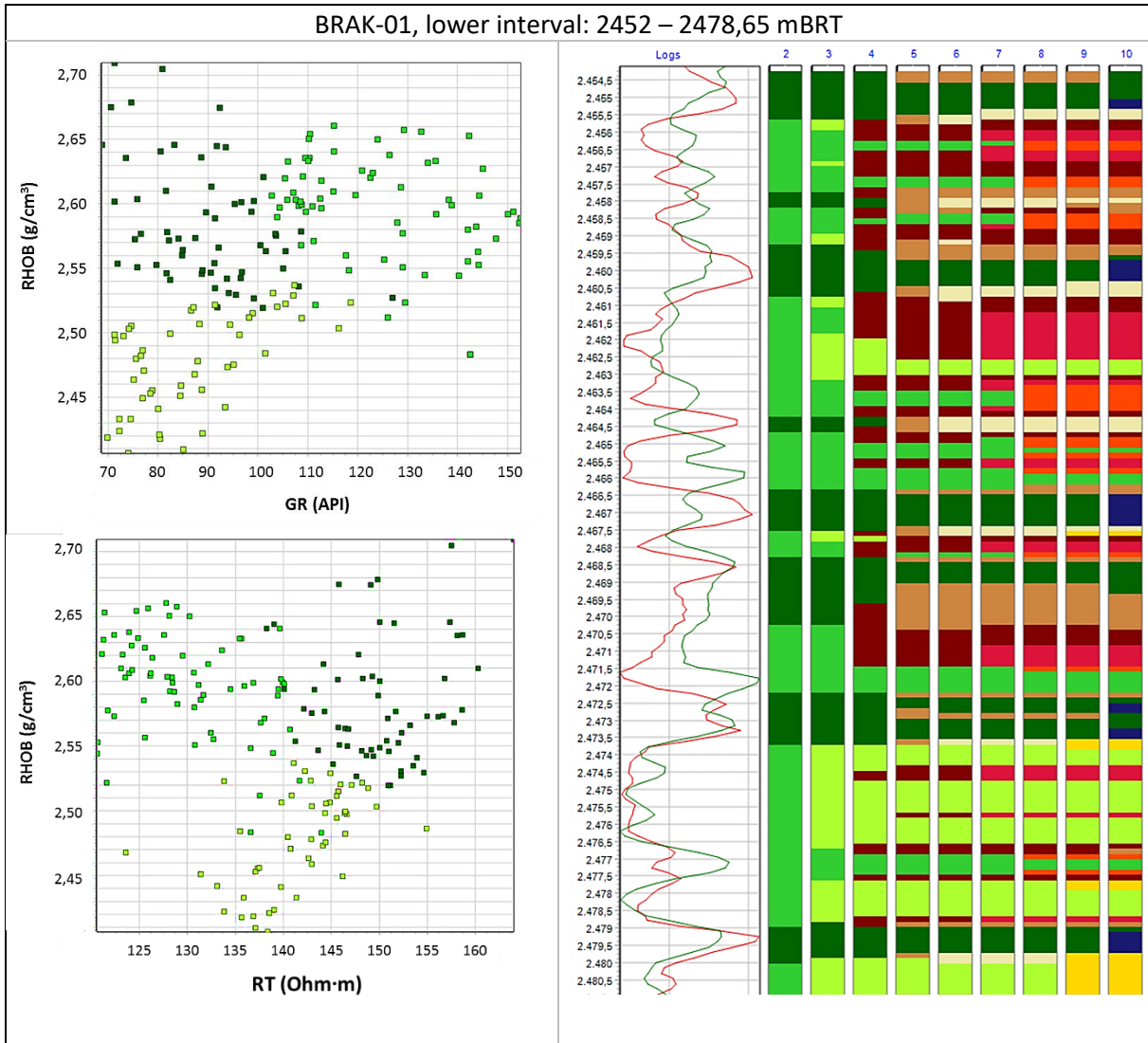


Figure 13: Results of Wkmeans modelling for the lower interval of BRAK-01. (A) and (B): Wireline data with their corresponding cluster. The number of clusters (i.e. 3) corresponds to the optimum derived from the PFS plot. (C): Distribution of clusters along the borehole interval. Each column represents the number of clusters, starting from 2. (D): PFS plot with the optimum number of clusters.

5.2.2 KDK-01

For this well, two intervals have been used for electrofacies analysis. The lower interval lies within the RBMVL (Lower Volpriehausen Sandstone Member). The upper interval lies within the RNROF (Röt Fringe Sandstone Member) and the RNROY (Upper Röt Fringe Claystone Member).

Lower interval (fig. 14)

The deepest interval runs from 2258 to 2275,10 mBRT. The interpreted lithofacies from GAPS, 1992 are (1) floodplain with minor fluvial channels and (2) braided channel complex.

The input for the electrofacies analysis are the gamma ray log (GRCGAPI), resistivity log (RTOHMM) and the porosity (PHIDEDITDEC). The best fit is found at 2 clusters. The electrofacies matches well with the interpreted lithofacies.

Upper interval (fig. 15)

The upper interval of KDK-01 runs between 1944 and 1981 mBRT. The interpreted lithofacies are (1) sheetfloods / distal alluvial fan, (2) floodplain, (3) braided channel complex, (4) abandoned channel / overbank, (5) floodplain with ponds/lakes and minor channels and minor soils, (6) floodplain pond/lake.

As input for the clustering, the following logs are used: gamma ray (GRCGAPI), resistivity (RTOHMM), porosity (PHIDEDITDEC). The statistical best fit for the clustering yields 2 to 4 clusters. Some of the facies interpretations match very well with the electrofacies results, for example the braided channel complex and abandoned channel/overbank. The braided channel complex shows high porosity and permeability values and low resistivity measurements, as well as a low gamma ray response.

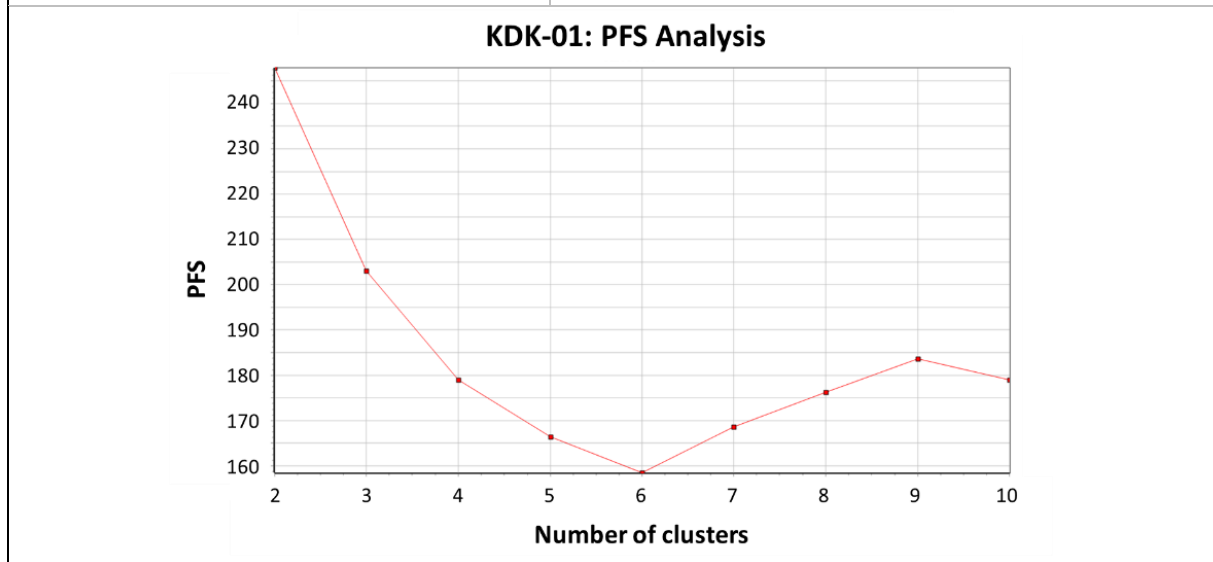
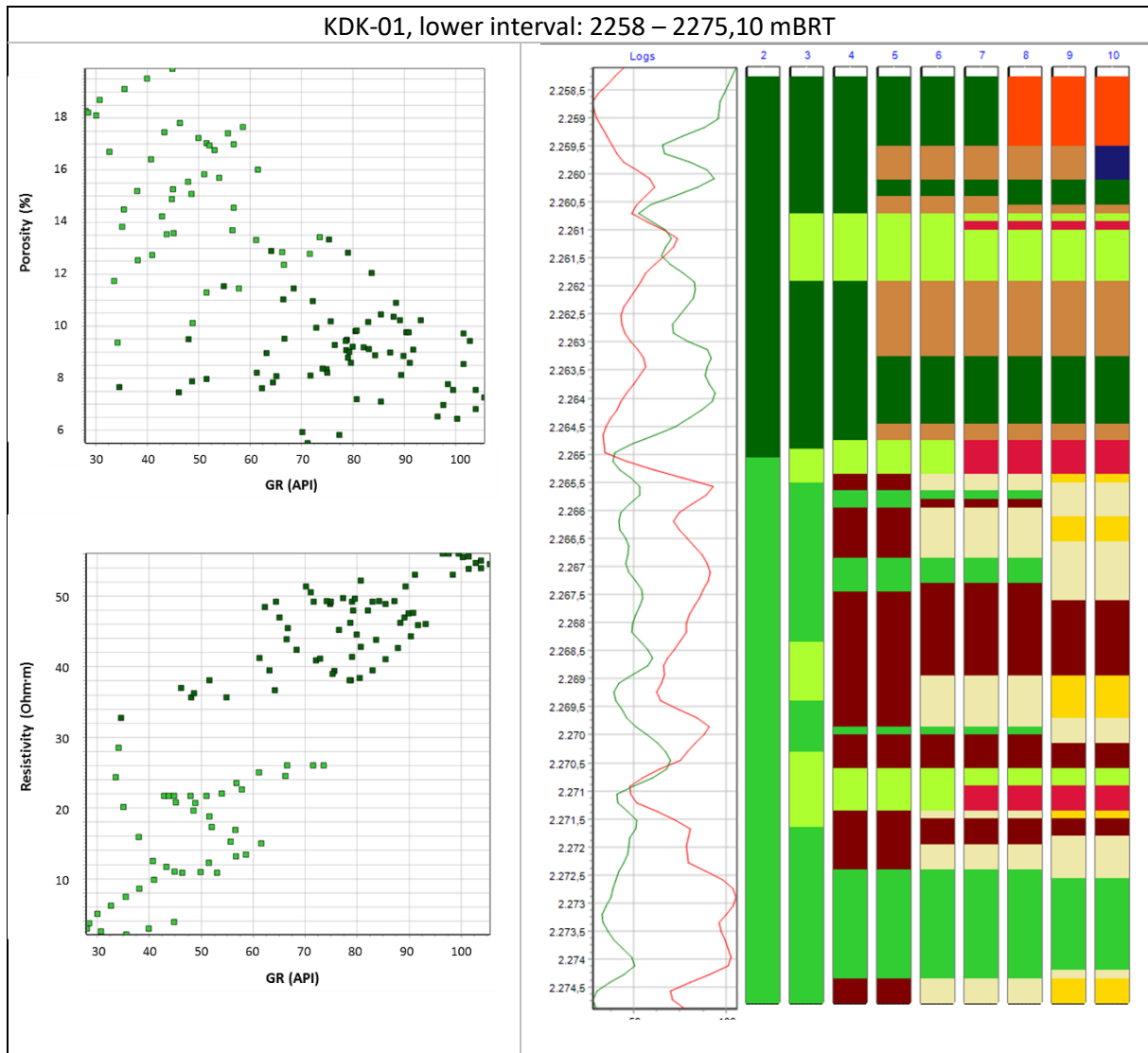


Figure 14: Results of Wkmeans modelling for the lower interval of KDK-01. (A) and (B): Wireline and core plug data with their corresponding cluster. The number of clusters (i.e. 2) corresponds to the optimum derived from the PFS plot. (C): Distribution of clusters along the borehole interval. Each column represents the number of clusters, starting from 2. (D): PFS plot with the optimum number of clusters.

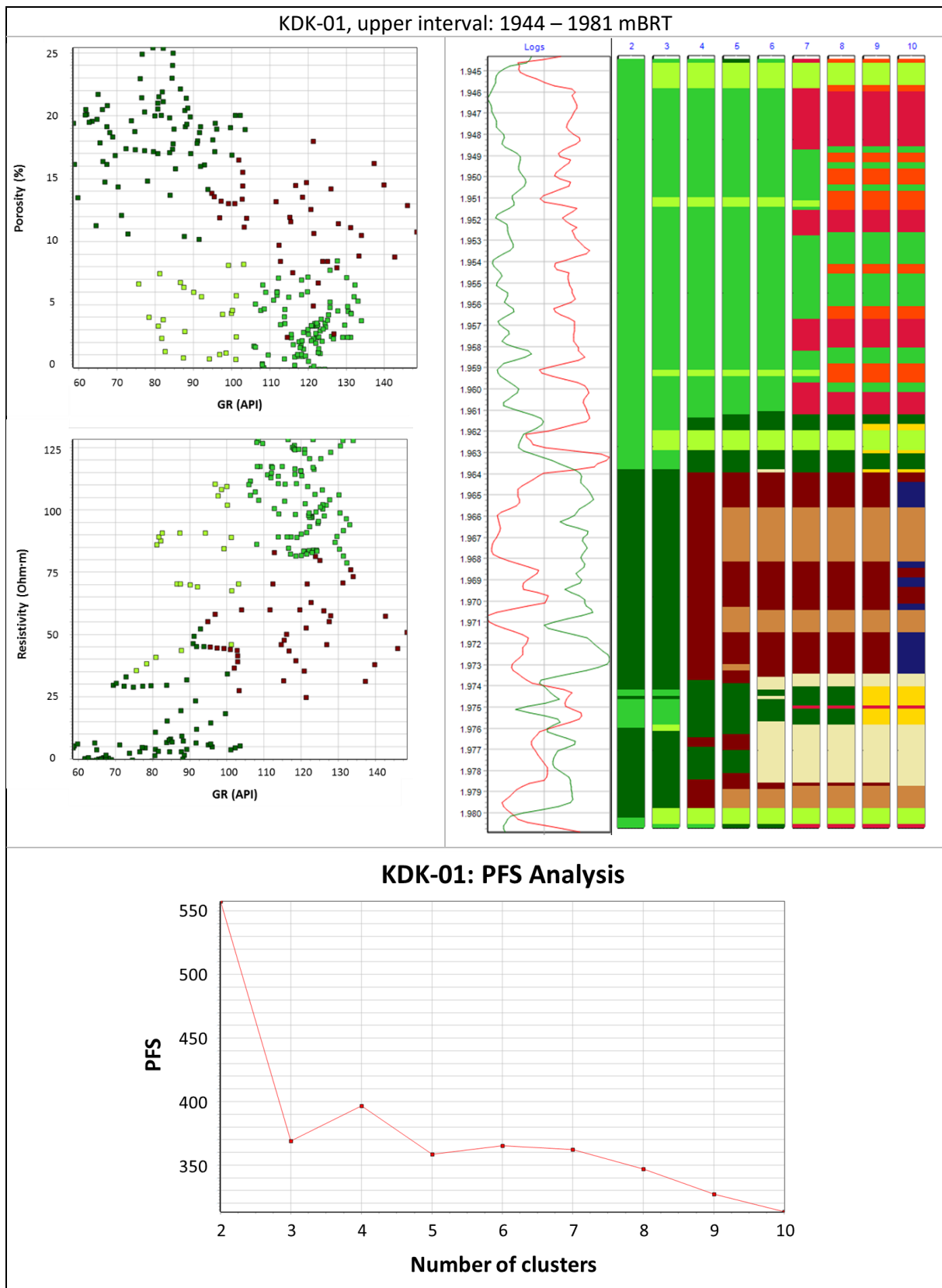


Figure 15: Results of Wkmeans modelling for the upper interval of KDK-01. (A) and (B): Wireline and core plug data with their corresponding cluster. The number of clusters (i.e. 4) corresponds to the optimum derived from the PFS plot. (C): Distribution of clusters along the borehole interval. Each column represents the number of clusters, starting from 2. (D): PFS plot with the optimum number of clusters.

5.2.3 WWK-01 (fig. 19)

The interval lies within the RNROF (Röt Fringe Sandstone Member) and the RNROY (Upper Röt Fringe Claystone Member). The interval between 3470 and 3518 mBRT has been analyzed. The sedimentology report by BP distinguishes 2 main lithofacies, a sandy and a shaly one. The sand lithofacies is composed of 5 minor sub-facies: (1) mica-rich sandstone, (2) scour surface on mudstone, (3) cryptic scour surface, (4) sandstone with mud clasts, (5) sandstone. The mudstone lithofacies contains two sub-facies: (6) silty mudstone and (7) mudstone. Three stacked sequences of facies 1 to 7 have been distinguished from the core analysis.

The input for the clustering comprises the gamma ray (GR), effective porosity (PHIE) and the bulk density (RHOB). A core shift of approximately 2 to 3 m provides a better fit with measured permeability values. The three stacked lithofacies associations are clearly separated by shaly intervals at the top of the sequence. This is reflected by the GR, porosity, permeability and bulk density. The electrofacies clustering results reflect this shaling-up trend rather well. The PFS plot shows that the best fit is found at 3 clusters. For this interval the clusters are likely matched to a lithofacies of sand, shale and a combined sand-shale facies.

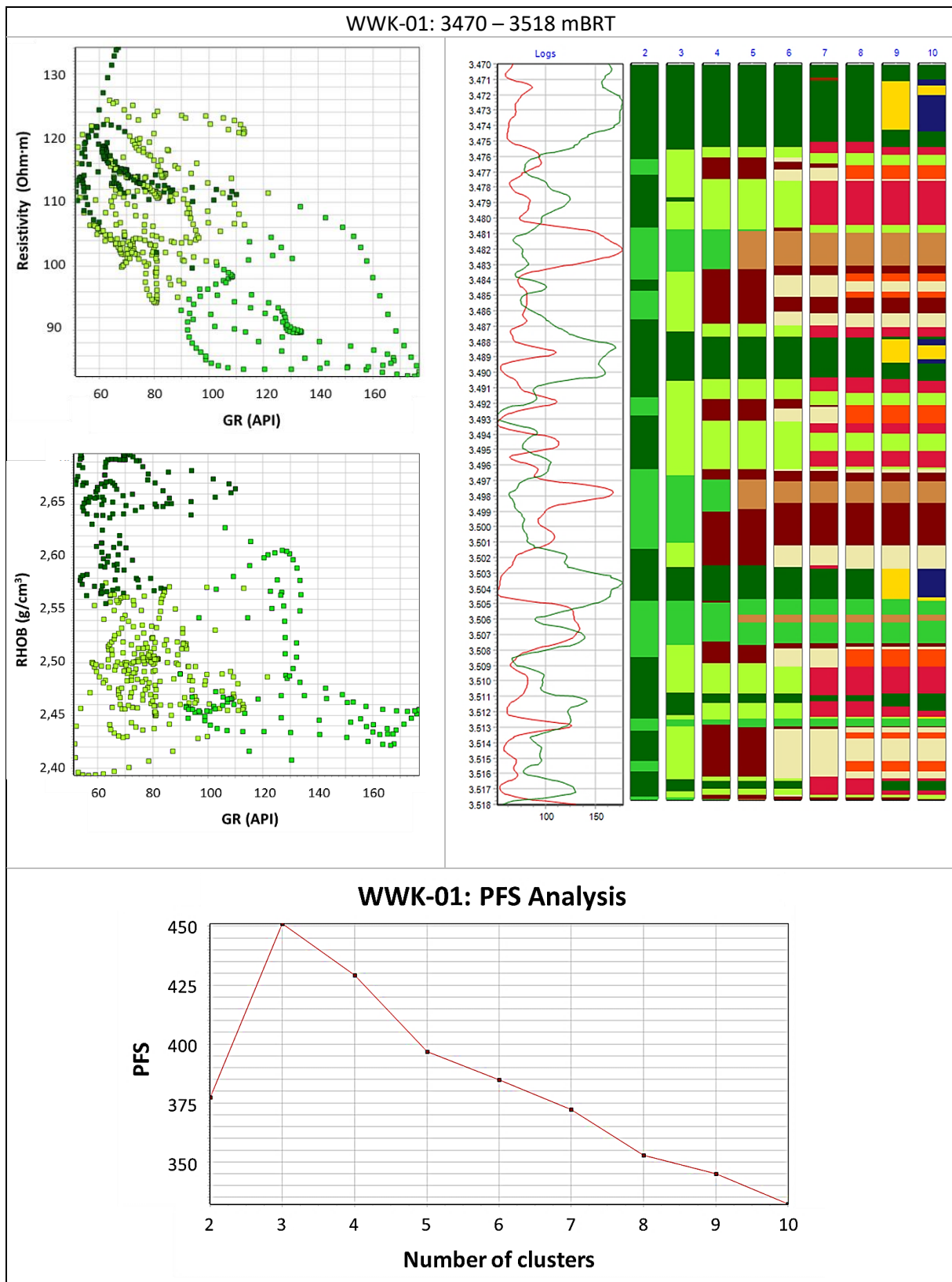


Figure 16: Results of Wkmeans modelling for the lower interval of WWK-01. (A) and (B): Wireline data with their corresponding cluster. The number of clusters (i.e. 3) corresponds to the optimum derived from the PFS plot. (C): Distribution of clusters along the borehole interval. Each column represents the number of clusters, starting from 2. (D): PFS plot with the optimum number of clusters.

5.2.4 WWS-01-S1 (fig. 17)

The interval lies within the RNROY (Upper Röt Fringe Claystone Member). Here a 6,5 m interval between 3109 and 3115,50 mBRT has been analyzed. The three interpreted depositional environments are (1) fluvial channel, (2) desert lake with occasional inland sabkha conditions and (3) distal sheetfloods in desert lake.

The input for the k-means clustering contains the gamma ray log (GRC), the bulk density log (RHOBEDIT) and the resistivity (RT). The PFS (Pseudo F-statistic) indicates a best fit at 7 to 19 clusters. However, this is not reflected by the facies, of which there are only 3 interpretations. The large number of clusters may be the result of an insufficiently large data set over the 6,5 m interval. The facies are the best distinguished by the resistivity log and porosity measurements from core plugs, where the fluvial channel shows an increased porosity up to 7% and increased resistivity. The desert lake with sabkha conditions is characterized by anhydrite, which is indicated by the presence of the high density (2.95 g/cm³) grains and it is mentioned in the sedimentary log.

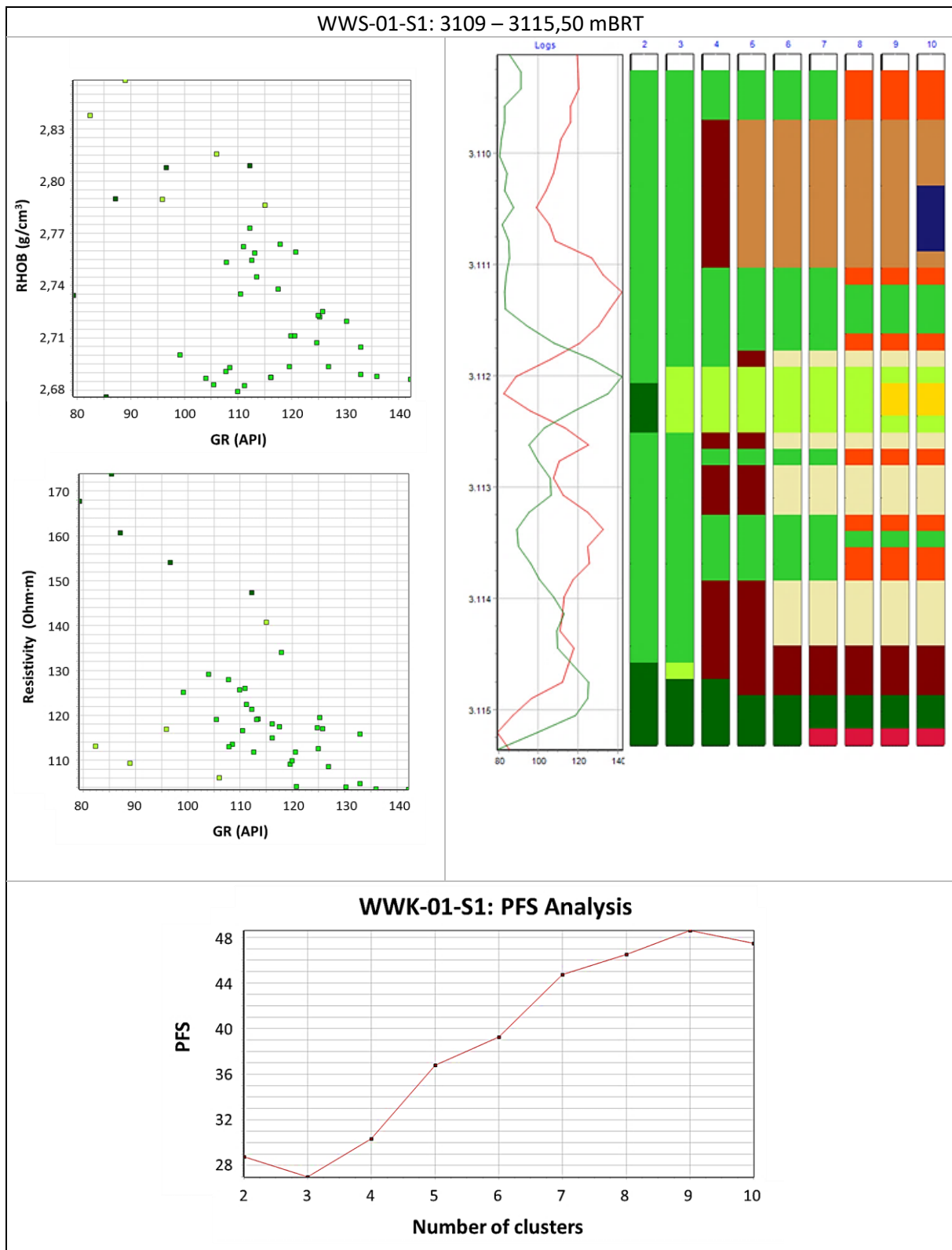


Figure 17: Results of Wkmeans modelling for the interval of WWS-01-S1. (A) and (B): Wireline data with their corresponding cluster. (C): Distribution of clusters along the borehole interval. Each column represents the number of clusters, starting from 2. (D): PFS plot with the optimum number of clusters.

5.3 Lithology prediction in Petrel

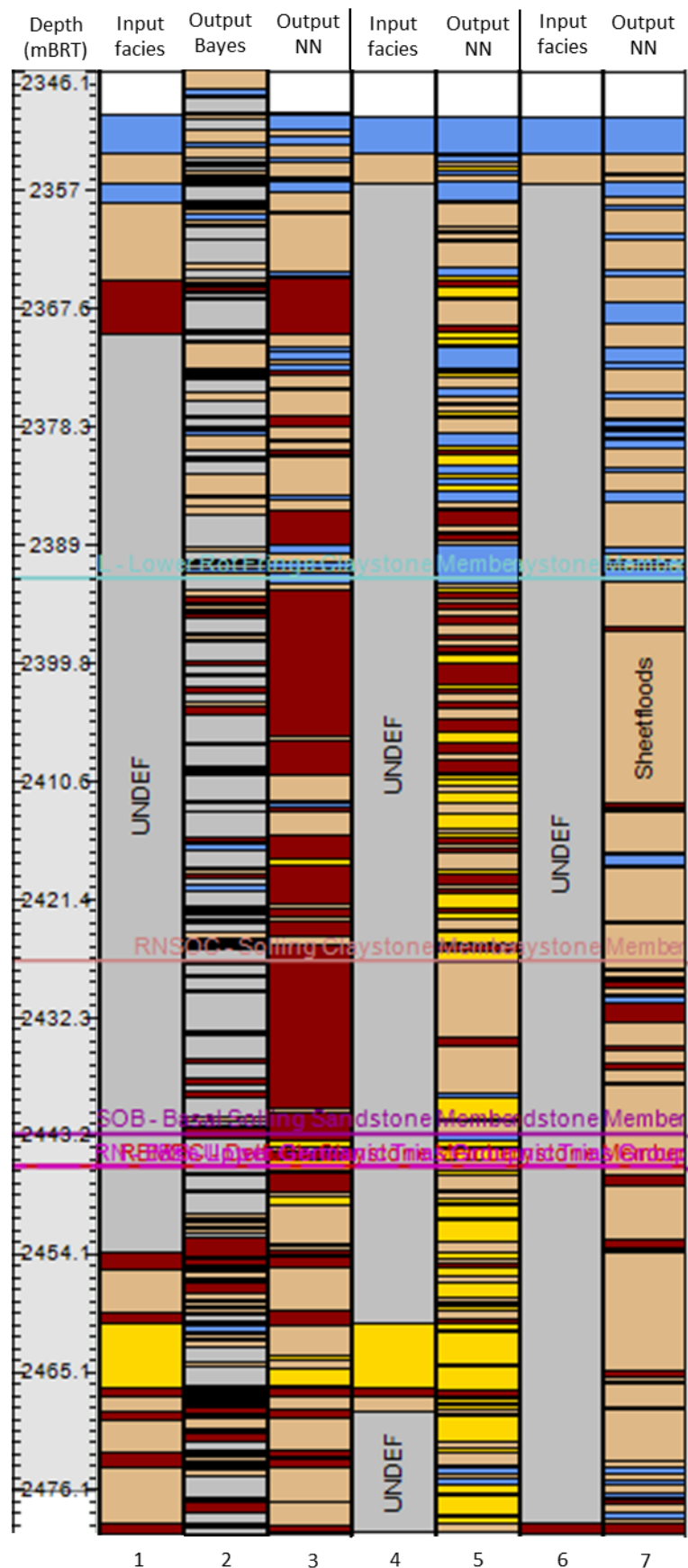
The results of the lithofacies modelling in Petrel will be shown here. The lithology predictions in the wells are shown in this section. The probability density functions (PDFs) have been added as appendices. Lithology prediction has been performed on the wells BRAK-01, KDK-01, WWN-01-S2. Wells WWK-01 and WWS-01-S1 have been excluded from the modelling. The available lithofacies description for well WWK-01 is from a much lower level of detail compared to the other wells. Because of the uncertainties related with the input facies, further modelling would not produce reliable estimates. The interpreted facies interval for WWS-01-S1 is too short (i.e. 6,5 m) to produce meaningful lithology predictions.

5.3.1 BRAK-01 (fig. 18)

All available wireline logs have been used as input, i.e. GR, NPHI, RHOB and DT. The upper interval of 20 m runs from 2349 – 2369,10 mBRT. The lower interval of BRAK-01 is located at 2452 to 2478,65 mBRT. After careful analysis of the wireline and core response, a core shift of 2 MD downwards has been applied. This means that the logs of the horizontal permeability, porosity and grain density are shifted downwards relative to the wireline logs. The panels show the final result of the modelling. The first panel shows the interpreted facies intervals from the lithological log which serves as the input for both the probabilistic and neural

Name	Background
Sheetfloods	
Fluvial channel	
Floodplain pond	
Abandoned channel/overbank	
Braided channel complex	
Floodplain with minor fluvial channels	

Figure 18: Results of the lithofacies modelling of well BRAK-01. Panel 1: input. 2: output probabilities. 3: Output neural net. 4: decreased input. 5: new output neural net. 6 & 7 are also new input and output.



prediction. The second panel shows the result of the lithofacies prediction from probabilities. The third panel shows the result of the lithofacies prediction from the neural net. When a shorter interval is used as input (panel 4), the neural prediction (panel 5) differs largely from the previous prediction (i.e. panel 3). This method has been applied another time.

When the uninterpreted intervals in the input pane are marked as 'UNDEFINED', the neural net is able to predict these intervals too.

The probability density functions (PDFs) can only be produced for lithofacies which input contains at least 2 separate intervals. Here PDFs are available for (1) Sheetfloods, (2) Fluvial channel and (3) Floodplain pond. PDFs are shown per attribute, i.e. GR, NPHI, RHOB and DT.

Plotting a poroperm from the available core plugs with their interpreted lithofacies does not yield a better facies distinction. The porosity-depth plot is does not show a clear facies distinction either.

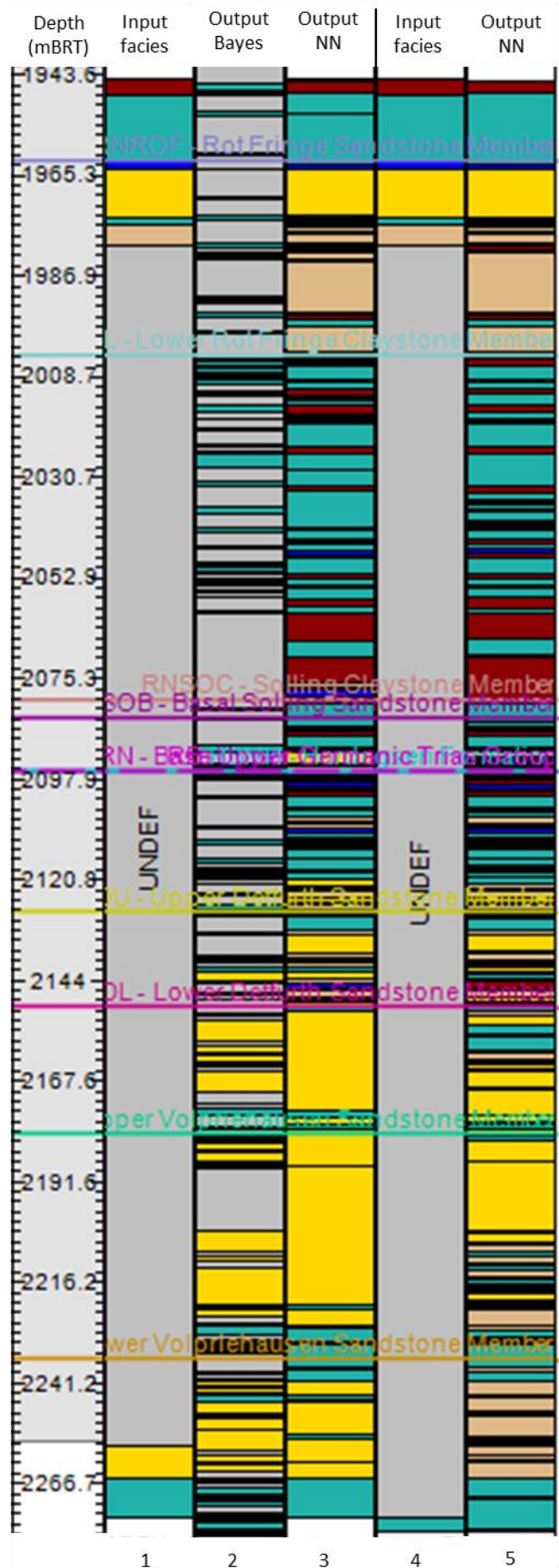
5.3.2 KDK-01 (fig. 19)

The wells used for litho-analysis are GR, RHOB and RESD. The deepest interval runs from 2258 to 2275,10 mBRT and the upper interval between 1944 and 1981 mBRT. The input panel shows the intervals with (1) Sheetfloods, (2) braided channel complex, (3) floodplain with minor fluvial channels, (4) abandoned channel/overbank and (5) floodplain pond. The lower interval only contains the braided channel complex and the floodplain with minor fluvial channels. Therefore PDFs of only these two facies are created. As an example, the PDFs can be shown for 1, 2 or three attributes in comparable dimensions.

The lithology prediction based on these PDFs is shown in panel 2. The neural net prediction is shown in panel 3.

The validity of the neural net prediction within the well is tested as follows. The upper interval as derived from core interpretation is used as input, as well as a small interval below. The neural net then predicts a sequence (panel 5) that is very similar to the first prediction. A close-up of the lower interval shows the predictions in more detail. The floodplain with minor channels facies is predicted very well and is a continuation of the assigned interval. The braided

Figure 19: Results of the lithofacies modelling of well KDK-01. Panel 1: input. 2: output probabilities. 3: Output neural net. 4: decreased input. 5: new output neural net.



channel complex is not recognized as such, but as a sheetflood sequence. Although it is a different lithofacies, there is some resemblance in the log responses from both.

The output facies that has been linked to the data can be used for further analysis, such as the occurrence within the porosity-permeability space. The poroperm (Appendix III) shows a rather good distinction between the braided channel complex and the floodplain with minor fluvial channels. The other facies do not show a distinct trend, possibly due to the low number of data points.

The porosity-depth plot (Appendix III) shows a large spread in the facies. The braided channel complex plots on the higher side of the porosity, whereas the floodplain with minor fluvial channels shows on the lower porosities. The floodplain pond has a low number of data points, but plots on the low side of porosity. The neural net prediction can also be visualized in for example a plot of gamma ray versus resistivity (fig. 20). The results of the lithofacies modelling show an improved distinction into separate groups.

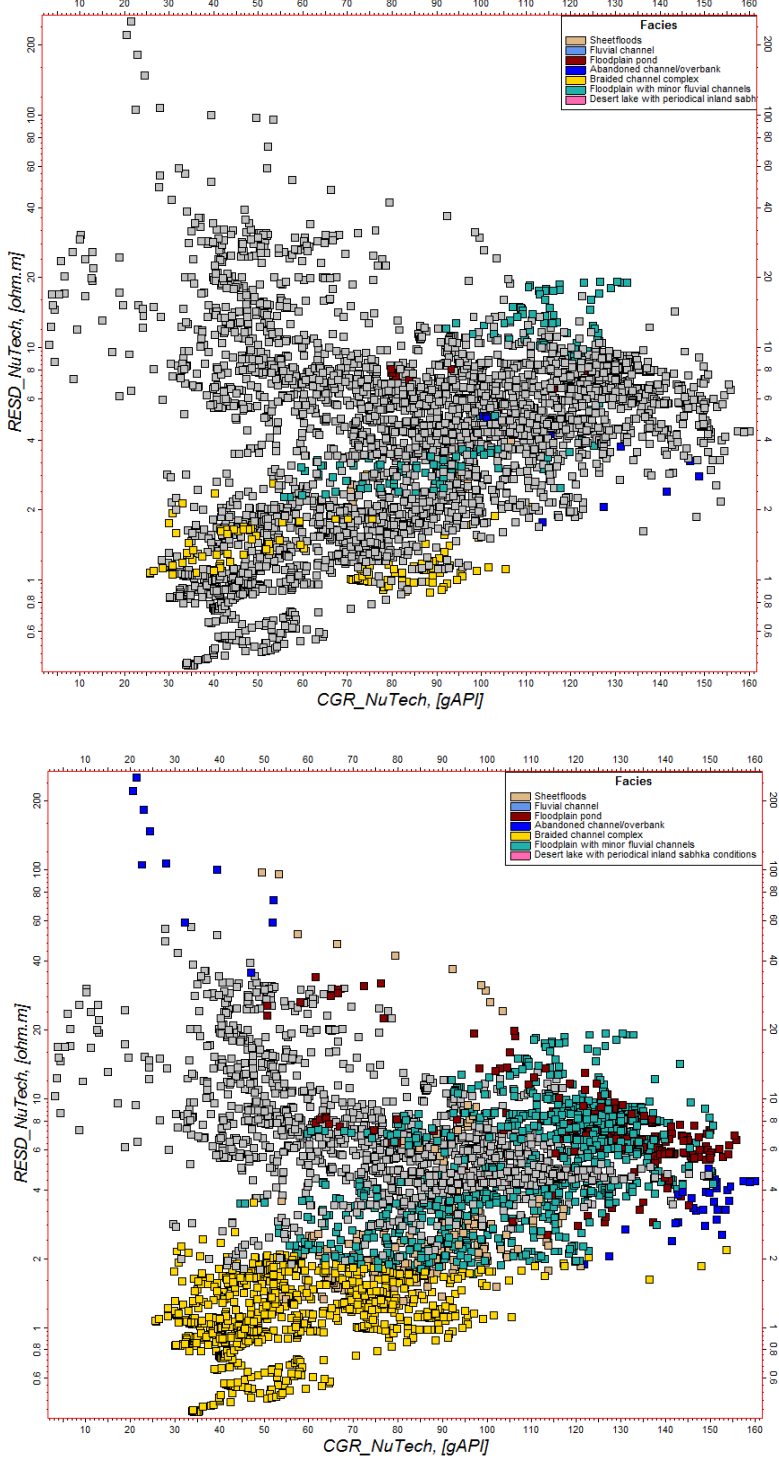


Figure 20: Data cloud of gamma ray (CGR_NuTech) versus resistivity (RESD_NuTech) of well KDK-01. (A): Colored squares correspond to the input facies, grey squares correspond to undefined intervals. (B): Colored squares correspond to the output facies, grey squares correspond to undefined intervals.

5.3.3 WVN-01-S2 (fig. 21)

The interval between 3305 and 3169 mBRT has been analyzed. The interval lies within the following members: RBMVL, RBMVU, RBMVA, RBMDU, RBMH. For this well, the total of wireline logs is limited to the gamma ray and the sonic log. Besides the wireline logs, abundant core plug data is available along the interpreted interval. Panel 1 in figure 21 represents the facies interpretation from the cores. Due to the limited number of wireline logs, a different approach has been used for this well. Here, the input is not the wireline logs but the plug data: porosity, horizontal permeability and grain density. The results of neural net prediction are shown in panel 2. Since the panel showed a large number of discontinuities, the input log had to be improved. Therefore the porosity, permeability and grain density logs were interpolated where possible. The interpolation was applied in a rather conservative way to prevent further uncertainties. The interpolated logs were input for the neural prediction, with the results visible in panel. Although a clear improvement, a large number of undefined intervals remained.

Therefore the input logs were changed to the wireline logs, i.e. gamma ray and sonic. Panel 4 shows the resulting facies prediction from the probabilities of the wireline. The associated PDFs have received more than two intervals per lithofacies, which means that there is sufficient input for both the PDF calculation as well as the lithology prediction. However, the resulting panel varies significantly from the input facies.

Panel 5 shows the lithology prediction of the neural net, and this shows a better match between the input and modelled facies.

The poroperm plot does not show a better distinction of lithofacies.

The porosity-depth plot shows good clustering for the floodplain pond facies, and slightly for the braided channel complex. The sheetfloods and floodplains with minor fluvial channels show no clustering.

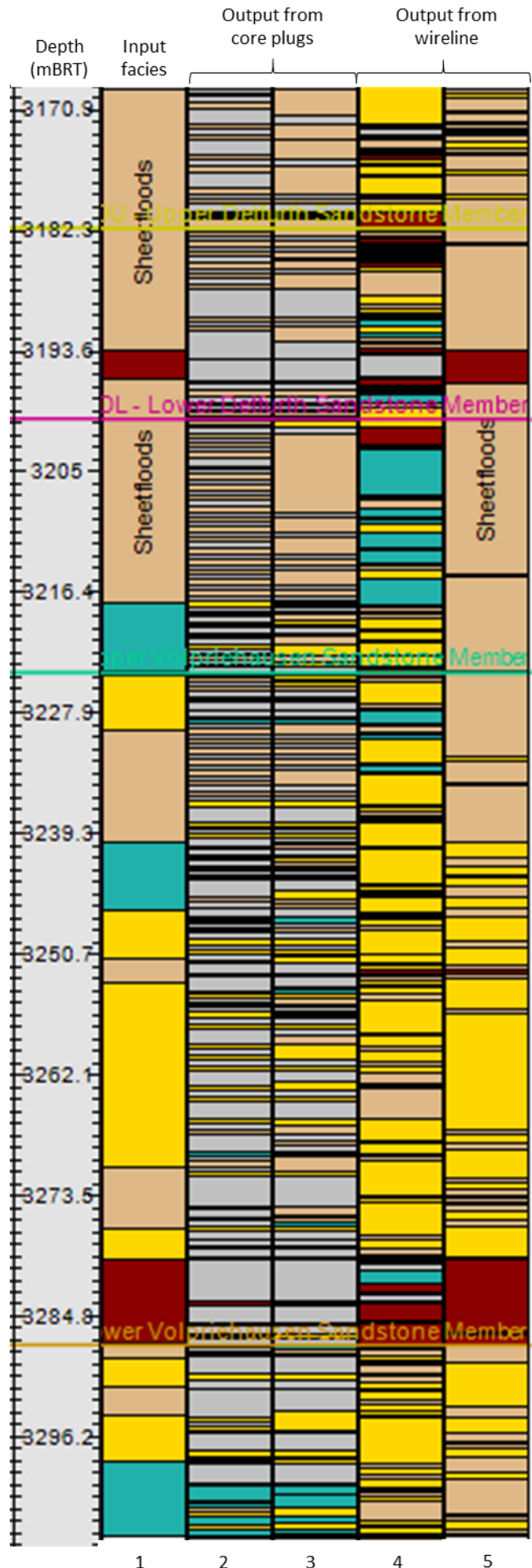


Figure 21: Results of the lithofacies modelling of well WVN-01-S2. Panel 1: Input. 2: Output from core plugs with neural net. 3: Output from interpolated core plugs with neural net. 4: Output from wireline data with Bayes method. 5: Output from wireline data with neural net.

6. Discussion

First the individual results of the cluster analysis and Petrel predictions will be discussed. Furthermore the methods themselves will be discussed. A reflection on the research question will be provided, while previous studies are discussed as well.

The contribution of this project to theory and practice is discussed here too. The limitations of the study are considered as well.

6.1 Cluster analysis in Wkmeans

Here the results of the k-means clustering are discussed with respect to the applicability to facies determination. Possible explanations for good and poor correlations will be discussed.

6.1.1 BRAK-01

In the upper interval from 2349 – 2369,10 mBRT, the best match between the clustered electrofacies and the depositional environment is from floodplain ponds/lakes, which show a distinct increased gamma ray and bulk density and lower resistivity. These observations are in line with the typical behavior of clays, with tightly packed conductive minerals.

The lower interval from 2452 – 2478,65 mBRT shows a very good correlation of the sheetflood ponds/lakes, which can be linked straight from the clusters to the facies interpretations for all 6 pond intervals. However, when considering 3 facies, a mismatch arises in the sheetfloods facies and the channel facies. The cluster of the lowest interval of stacked sheetfloods reappears in thin bands within the cluster of sheetfloods with minor channeling. This reappearance occurs within three different sheetflood interval, except for the homogeneous sheetflood interval. Furthermore the lower stacked sheetfloods show a distinct increased permeability. Given these arguments, the clustering indicates a revision of the interpreted facies for the lower stacked sheetfloods, pointing towards a channel environment. A revision of the log description is needed to consider the possibility of a braided channel complex, rather than stacked sheetfloods. Core photos and the log description show minor cross bedding in the braided channel complex, whereas the bedding appears more planar parallel in the stacked sheetfloods interval. Therefore the lithofacies interpretation is not changed after cluster analysis.

6.1.2 KDK-01

For the upper interval (1944 – 1981 mBRT), the clear match between the electrofacies and interpreted depositional environment can be contributed to all logs recording the change in lithology. Therefore this is a good example for the use of electrofacies modelling.

The lower interval from 2258 to 2275,10 mBRT contains a much more complex sequence, although the major trends are properly recognized by the cluster analysis. The braided channel complex stands out the most from the other facies.

6.1.3 WWK-01

For the interval between 3470 and 3518 mBRT, there appears to be a good match between logs, cores and electrofacies interpretation. The triple stacked lithofacies association of a shaling up sand sequence from the interpretation is reflected in detail by numerous logs, creating strong relations and distinct clusters. The particular stacking or repetition of the sequences makes this interval particularly useful for comparison.

6.1.4 WWS-01-S1

The poor fit of the gamma ray log with the depositional environments could be due to a core shift. As this interval is only 6,5 m (between 3109 and 3115,50 mBRT), a core shift might disturb the image and yield no relevant insights.

However, the resistivity log and plug porosities do indicate the facies accordingly, so a core-log mismatch is not expected. Here, the mere gamma ray log may be a poor indicator for facies, as mentioned by (Rider, 1990). When GR is omitted from the clustering, it still does not lead to a better fit with the facies interpretations. Perhaps more data in this interval or a longer interval is required to create geologically better clustering.

6.2 Lithology prediction in Petrel

Here the results of the lithology prediction in Petrel will be discussed and interpreted. Furthermore limitations and prerequisites of the technique are discussed.

6.2.1 BRAK-01

The lithology prediction from probabilities has yielded a very incomplete facies sequence with many undefined intervals. Even the two interpreted intervals are poorly reproduced by the probability technique. The wide range in the Probability Density Functions causes the poor correlation. Moreover the braided channel complex is lost entirely from the prediction, due to its single occurrence in the input facies panel.

The prediction from the neural net (panel 3) shows a good match with the predefined interval. The predicted lithofacies between the lower and upper interval appear to match the log response seen in the interpreted intervals.

For neural net prediction, at least one interval per lithofacies is required. Because the upper and lower interval each contain a unique facies, a check between intervals is not possible. Shorter input intervals give varying results. Generally, the shaly intervals are best recognized as floodplain ponds/lakes. Extrapolation of the neural net to the base of the Triassic (RBSH) indicates the presence of braided channel complexes in the RBMVU. This interval is characterized by a low serrated gamma ray signal, associated with a sequence of channels and barrier bars (Rider, 1990; Serra, 1983). Correspondingly, the core interpretation of the RBMVU in well WVN-01-S2 indicates a braided river complex. Furthermore the neural net indicates a braided channel complex in KDK-01. Therefore this prediction appears to be valid, which makes this interval interesting for further investigation.

The poor facies clustering from the poroperm and porosity-depth plot does not allow for a better facies distinction in this well, so more data might be beneficial.

In this case, the best results are obtained from the neural net with wireline logs. The core data shows poor clustering, making it difficult to make any predictions.

6.2.2 KDK-01

Due to the presence of two interpreted facies intervals, this well is suited for a proper quality control of the lithology prediction. The prediction from the PDFs, the probabilities, is clearly insufficient; the panel contains a large amount of discontinuities within the predicted interval and outside. The lithofacies prediction of the neural net has a good match with the interpreted facies intervals. Given that a smaller input yields a similar result, the neural net is considered very successful in this particular well interval.

The poroperm shows a rather good facies distinction between at least two different facies, with the braided channel complex being the most distinguished in the upper right corner of the poroperm trend.

The porosity-depth plot does not show a good facies clustering, so more data is required.

6.2.3 WVN-01-S2

Predictions from core plugs have proven to be problematic, since a large amount of interpolation is required. The advantage of wireline logs over core logs is that they are continuous measurements, whereas the core logs are point measurements. This problem cannot be overcome completely, but an approximation of porosity is possible from calculating a porosity from the bulk density and the grain density, followed by taking the root mean square of this calculation and the neutron porosity. Unfortunately, the required RHOB and NPHI logs are absent in this well.

The other option is the use of the two wireline logs. The probability density functions show that the different facies appear very similar in their log responses, especially for the sonic. Consequently, the resulting lithology prediction shows a poor facies relation with the interpreted interval.

The best match comes from the neural net prediction based on the wireline logs. However, in this prediction one facies has been omitted: the floodplain with minor fluvial channels is not recognized by the neural net.

For this interval, the poroperm plot does not show an improved lithofacies distinction.

Since the porosity-depth plot only shows good clustering for the floodplain pond facies, the results are not useful for predicting facies elsewhere.

6.3 Property maps

The cluster analysis and lithology prediction were means to improve the current mapping methodologies by using the electrofacies or log response per facies. Here the methodologies of the property maps will be discussed as well as the implications of the new electrofacies approach. Regional porosity maps exist for the West Netherlands Basin (Vis et al., 2010) and for the entire Netherlands (including offshore) in 2017. Both map projects were based on porosity data from wells, although different driving maps were used; respectively maximum burial depth and facies. The advantages and disadvantages of both approaches will be reviewed. Given that both studies delivered a porosity map for the West Netherlands Basin, comparison of the output maps would provide a good visual comparison of different methods. However, the 2010 study contains a map of all Triassic intervals stacked, whereas the 2017 study shows porosity maps per member, making this an invalid comparison. Therefore the results of the mapping projects will not be evaluated, but rather the methodology that underlies the property maps. Finally the methodology of the new electrofacies approach will be discussed.

Other studies have not been able to combine facies with determining poro-perm relationships in the Roer Valley Graben. Appointing facies to poro-perm data did not result in a better separation of clusters, hence facies was not incorporated in the poro-perm relations (Maaijwee et al., 2012). A better clustering in poro-perm relations has been established based on grain densities rather than facies, at least for the Lower Volpriehausen Sandstone Member RBMVL (Van Kempen et al., 2018).

6.3.1 Maximum Burial driven

The TNO porosity maps from 2017 used core and log data and extrapolated the values based on the porosity-depth relation. In other words, these property maps are conditioned on the maximum burial depth. When starting with the creation of a regional porosity map, the porosities measured in the wells are plotted against their depths. The trend arising from this plot is used with a maximum burial depth map, which assigns the expected porosity with the particular depth.

An advantage of this method is that the maximum burial can be rather well determined. Since the Roer Valley Graben does not have a significant burial anomaly, the present day depth can be regarded as the maximum burial depth (Nelskamp & Verweij, 2012). Present day depths can be traced as horizons from seismic data, so even some distinction between major lithological markers can be established.

A disadvantage is the generally poor relation between maximum burial and porosity due to initial facies variations and secondary diagenetic processes. In order to select only the good reservoir, intervals with a high clay content or with diagenetic influences must be excluded. When this is done consistently, a strong poro-depth relation emerges from the dataset (Van Kempen et al., 2018). However, this trend is only validated for measurements based on grain density, a property that can only be obtained from cores and not from wireline data. Wireline only measures bulk density (RHOB), which is a combination of matrix density, porosity and pore fluids. Regardless of this finding, it remains very difficult to derive local porosity estimates from a regional porosity-depth trend.

6.3.2 Facies driven

For the West Netherlands Basin a property map has been constructed with a driving map based on facies (Vis et al., 2010). Here the porosity and permeability data from cores have been linked to facies. A classical facies modelling algorithm kept the facies fixed in the wells, while varying them outside of the wells. Repeated runs finally resulted in an statistically averaged 3D facies model.

A disadvantage is the difference in information between wireline data (logs) and cores. Since only a few select intervals are sampled for cores and plugs, the rest of the well is evaluated only by wireline measurements. In general, wireline data is used to determine sand/shale cutoffs, followed by facies modelling in the reservoir sands. Especially when interpreting lithofacies without cores and plug data, the uncertainties increase.

A second disadvantage is the loss of detail that occurs with upscaling. The facies modelling uses a 'most of' criterion, causing thin facies intervals to be occluded by the thicker intervals. However, the transmissivity of a potential reservoir is largely determined by the preferential flow of high perm intervals, which can be very thin (Pluymaekers et al., 2012). When these thin but high perm intervals are excluded from upscaling, the modelling will result in overly pessimistic outcomes. According to Walther's Law, facies that are stacked conformably on top of each other, can also be found laterally to each other. Therefore it may be possible that the thin high perm intervals measured in the well are pinch outs of much thicker intervals further away from the well.

An advantage of this method is that it agrees with the general finding that facies is the most important factor controlling reservoir quality (K18-Golf Unit, 2016). Hence, a solid facies model of the Triassic is essential in determining the reservoir potential of the Roer Valley Graben.

Further analysis of the methodology by Vis et al., 2010 has shown the following. For wells and intervals with only wireline data, the sand-shale intervals were interpreted based on the gamma ray response. Facies modelling was then continued with only the sand intervals. Other logs than gamma ray such as sonic, neutron and density logs have been used in a cluster analysis to improve the sand-shale distinction. However, the other logs did not contribute to a better sand-shale separation, so the distinction between sand and shale in uncored intervals was based solely on gamma ray response. Only 5 out of the 77 wells in the West Netherlands Basin were used in the cluster analysis (Vis et al., 2010).

Some comments must be made with regards to the disappointing results of cluster analysis of Triassic intervals in the West Netherlands Basin. Only 5 out of the total of 77 wells have been used for cluster analysis based on gamma ray logs. Additionally, the use of only a GR log when distinguishing facies comes with limitations (Rider, 1990). That is, when solely relying on the GR log the mica-effect of sandstones might falsely indicate a shaly interval. Furthermore, the other logs also do not directly indicate sand and shale. Diagenesis and deeper burial both affect the porosity and mineralogy of the reservoir. Since the West Netherlands Basin has experienced more inversion and diagenetic processes than the RVG (Kombrink et al., 2012), it has a more affected porosity and permeability which in turn affect the NPHI and RHOB. This might explain the poor clustering results from these logs, as visualized by the extremely poor relation between permeability and burial depth (Vis et al., 2010). Cluster analysis may still prove useful for the RVG, especially considering the absence of a significant burial anomaly (Nelskamp & Verweij, 2012).

6.3.3 Exploring electrofacies

The porosity of a reservoir rock is controlled by three consecutive elements. The first and foremost control is facies. Next mechanical compaction and finally diagenesis affect the porosity. Therefore the present-day porosity may be the sum of all three processes.

A facies-driven porosity map has not yet been constructed for the Roer Valley Graben, only burial-driven property maps based on Van Kempen et al., 2018. It may be expected that these maps appear more or less similar: the deepest burial depth might match with a more shaly lithofacies, linked to the distal position of the basin away from the London Brabant Massif. The flanks of the structural highs surrounding the RVG are considered more proximal with coarse sediments associated with alluvial fans. A similar facies-depth trend has been identified in

the Middle to Upper Jurassic stratigraphic intervals of the northeastern North Sea (Ramm, 2000). Adjacent to this study area, this relationship is not as clearly present in the West Netherlands basin (Vis et al., 2010), whereas the Roer Valley Graben appears to be a much more 'intact' basin with less tectonic reactivation affecting the maximum burial depth. The absence of a significant burial anomaly in a basin setting supports preservation of the facies-depth relation.

Obviously, the main limitation on facies characterization in the Roer Valley Graben is the limited amount of data. There is a very limited number of wells with a wide geographical distribution and with only a few interpreted lithological intervals. This might explain why current schematic facies maps have such a high level of 'geo-fantasy' (Emery, 1987; Maaijwee et al., 2012; Winstanley, 1993). A combined approach is necessary to derive a more realistic facies distribution.

The goal of the electrofacies approach is to find particular combinations of log responses that provide a unique 'fingerprint' for a facies. Here the classification has been explored by either unsupervised and supervised classification, of which the latter is more preferable since it is easier to verify the validity of the model.

Cluster analysis as part of a statistical approach for lithology determination from well logs has been a widely used method (Geel & Lutgert, 1990). Previous studies have compared the predictions from standard statistics with the predictions from the neural net, with the latter giving the best fit (Rafik & Kamel, 2017; Wong, Jian, & Taggart, 1995). Predicting lithology from a neural net is not a new technique; it has been applied for more than two decades (Rogers et al., 1992), although often with varying results. However, with the present-day computational power and more publicly available data (e.g. the source of this study: NLOG), this method must be reconsidered for renewed potential.

Both the statistical approaches and the neural net workflow contribute to improving the existing property maps. In its current use, the neural net has proven especially meaningful. All of the existing facies maps have placed most of the studied wells from this study on the outer edge of an alluvial fan. However, interpretations of the lithofacies reports appear to indicate many floodplain ponds and sheetfloods. As this may hint at a more distal environment than previously suspected, further research would be beneficial.

The proposed methodology is focused on siliciclastic reservoirs only. Neither of the TNO mapping projects focused on the applicability of carbonate plays, despite the large lateral heterogeneity related to the occurrence of carbonate platforms. Further research is required to validate its use for carbonate reservoirs. With the current interest in carbonates for geothermal applications, e.g. the Dinantian carbonates, this might prove particularly useful.

7. Conclusions

The aim of this study was to improve the methodology for property maps of the Triassic formations of East Brabant. This has been done by (1) providing a detailed analysis of the current mapping methodologies and their limitations and (2) by introducing an additional lithology prediction analysis into the workflow. The following conclusions can be drawn:

- The property maps are the sum of facies, mechanical compaction and diagenesis, of which facies exerts the main control on reservoir quality. The main assumption for the Roer Valley Graben is that the distal low-energy sediments correspond to the most deeply buried parts of the basin, whereas the proximal high-energy sediments are deposited on the flanks of the surrounding highs (i.e. London-Brabant Massif and Rhenish Massif). This implies a strong relation between facies and maximum burial depth.
- Comparing the available core and log data it seems that diagenesis affects porosities very locally, making it very difficult to derive local porosity estimates from a regional porosity-depth trend. Moreover, local porosity variations are inherent to facies. The current Maximum Burial driven porosity maps are therefore not ideal.
- A supervised facies classification (as used in Petrel) is preferred over an unsupervised classification (Wkmeans) since it is easier to verify the validity of the model.
- With the current sparse data set, the best lithology predictions are made by the neural net rather than by the Bayes classifier.
- Despite their lower resolution, wireline logs are more favorable for lithology predictions than core plug logs, since they are not only in situ, but also continuous in depth.
- Neural net lithology predictions require sufficient input, i.e. enough interpreted facies intervals from cores. If this data can be acquired, an important enhancement in the accuracy of facies and related productivity predictions can be achieved.
- For the RVG study area, neural net lithology predictions are mostly a good indication for lithofacies within the same well. Extrapolation to other wells can be done, although the geological controls should always be properly accounted for.

8. Recommendations

The nature of the current interpolated property maps allows the reader to select an area of interest and retrieve an average porosity and permeability. Despite this being a very inviting way of retrieving information, potential users should recognize that this is also a major pitfall. Both geological and statistical uncertainties are not yet represented by the current property maps, making it difficult to assess the associated uncertainties. When using the maps in their current form, this should be emphasized to potential users, i.e. by specifying the boundary conditions for their proper use in a disclaimer. An alternative presentation of the data could be a separate or combined map with statistical and geological uncertainties.

To improve lithology predictions by neural nets in the future, sufficient amounts of input data are crucial. The combined suite of continuous wireline logs, tightly spaced core plug measurements and sufficient intervals with lithofacies interpretations from cores is necessary for improved machine learning. Although using all these techniques may not appear essential to a geothermal operator, this is the only way to improve our understanding of the geology in an area which is still sparse in recent wells. Moreover, with the current heated public debate on activities in the Dutch subsurface, every drilling opportunity should be used to its full extent as to collect as much data as possible.

The applied method of lithology prediction may prove to be more applicable in a more tightly covered area with more available interpretations. In that way the method may result in more meaningful predictions of regional lithofacies. Finally this method stresses that despite the enhancements with respect to machine learning, the input still requires the eye of the trained geologist or sedimentologist for the lithofacies and depositional environment interpretations.

9. Acknowledgements

I would like to thank my colleagues at EBN for their support, explanations and technical help, especially my supervisor Jan Lutgert, Marten ter Borgh, Walter Eikelenboom and Guido Hoetz. Besides conducting this research project, I enjoyed helping at the symposium on Ultradeep geothermal projects.

Many thanks to Fred Beekman for acting as my supervisor from Utrecht University, as well as being the organizer of the ISEC course which allowed me to gain useful Petrel experience.

The meeting I had in the early phase of my internship at the TNO office with Bart van Kempen, Maartje Struijk and Harmen Mijnlief greatly contributed to mastering the research question and methodology as applied. Bart Ursem is also thanked for his helpful insights from his project on the West Netherlands Basin.

Finally, I greatly value the warm support I received from my family and friends during my first internship and writing of this thesis.

10. References

- Athy, L. F. (1930). Density, porosity, and compaction of sedimentary rocks. *American Association of Petroleum Geophysicists Bulletin*, 14(1), 1–24.
- Barker, C., Pawlewicz, M., Buntebarth, G., & Stegena, L. (1986). The correlation of vitrinite reflectance with maximum temperature in humic organic matter. *Paleogeothermics*, 5, 79–93. <https://doi.org/10.1007/BFb0012103>
- Benedictus, T., Rijkers, R. H. B., & Witmans, N. (2007). Determination of petrophysical properties from well logs of the offshore Terschelling Basin and southern Central North Sea Graben region (NCP-2A) of the Netherlands. *Report TNO*, 1–53.
- Bjørkum, P. A., & Nadeau, P. H. (1998). Temperature controlled porosity/permeability reduction, fluid migration, and petroleum exploration in sedimentary basins. *Australian Petroleum Exploration Association Journal*, 38(1), 453–464.
- Bonté, D., Van Wees, J. D., & Verweij, J. M. (2012). Subsurface temperature of the onshore Netherlands: New temperature dataset and modelling. *Geologie En Mijnbouw/Netherlands Journal of Geosciences*, 91(4), 491–515. <https://doi.org/10.1017/S0016774600000354>
- Briere, P. R. (2000). Playa, playa lake, sabkha: Proposed definitions for old terms. *Journal of Arid Environments*, 45(1), 1–7. <https://doi.org/10.1006/JARE.2000.0633>
- Buik, N., de Jonge, H., & de Boer, S. (2016). *Potentieel geothermie in Zuid-Holland*.
- de Jager, J. (2007). Geological development. In *Geology of the Netherlands* (pp. 5–26).
- Emery, D. (1987). *The sedimentology and reservoir characteristics of the Middle and Upper Bunter Formations, Waalwijk-1, Onshore Netherlands*.
- Geel, C. R., & Lutgert, J. E. (1990). *Determination of lithofacies from well logs - first progress report*. TNO.
- Geluk, M. (2005). *Stratigraphy and tectonics of Permo-Triassic basins in the Netherlands and surrounding areas*. Faculty of Geosciences (Vol. Ph.D.).
- Geluk, M. C. (2000). Late Permian (Zechstein) carbonate-facies maps, the Netherlands. *Geologie En Mijnbouw/Netherlands Journal of Geosciences*, 79(1), 17–27. <https://doi.org/10.1017/S0016774600021545>
- Geluk, M. C. (2007). Triassic. In *Geology of the Netherlands* (pp. 85–106).
- Geluk, M. C., Duin, E. J. T., Duser, M., Rijkers, R. H. B., Van Den Berg, M. W., & Van Rooijen, P. (1994). Stratigraphy and tectonics of the Roer Valley Graben. *Geologie En Mijnbouw*, 73(2–4), 129–141.
- Glennie, K. W. (1998). *Lower Permian - Rotliegend*. *Petroleum Geology of the North Sea: Basic Concepts and Recent Advances: Fourth Edition*. <https://doi.org/10.1002/9781444313413.ch5>
- Hantschel, T., & Kauerauf, A. I. (2009). *Fundamentals of basin and petroleum systems modeling*. *Fundamentals of Basin and Petroleum Systems Modeling*. <https://doi.org/10.1007/978-3-540-72318-9>
- Hartigan, J. A. (1975). *Clustering Algorithms*. New York: Wiley.
- Kombrink, H., Doornebal, J. C., Duin, E. J. T., Den Dulk, M., Van Gessel, S. F., Ten Veen, J. H., & Witmans, N. (2012). New insights into the geological structure of the Netherlands; results of a detailed mapping project. *Netherlands Journal of Geosciences/ Geologie En Mijnbouw*, 91(4), 419–446. <https://doi.org/10.1017/S0016774600000329>
- Kramers, L., Van Wees, J. D., Pluymaekers, M. P. D., Kronimus, A., & Boxem, T. (2012). Direct heat resource assessment and subsurface information systems for geothermal aquifers; The Dutch perspective. *Geologie En Mijnbouw/Netherlands Journal of Geosciences*, 91(4), 637–649. <https://doi.org/10.1017/S0016774600000421>
- Kumar, V., Tan, P.-N., & Steinbach, M. (2005). Chapter 8: Cluster Analysis: Basic Concepts and Algorithms. In *Introduction to Data Mining*. [https://doi.org/10.1016/0022-4405\(81\)90007-8](https://doi.org/10.1016/0022-4405(81)90007-8)
- Lander, R. H., & Bonnell, L. M. (2010). A model for fibrous illite nucleation and growth in sandstones. *AAPG Bulletin*, 94(8), 1161–1187. <https://doi.org/10.1306/04211009121>
- Leeder, M. R., & Gawthorpe, R. L. (1987). Sedimentary models for extensional tilt-block/half-graben basins. *Geological Society, London, Special Publications*, 28(1), 139–152. <https://doi.org/10.1144/GSL.SP.1987.028.01.11>
- Maaijwee, C., Rombaut, B., & Buik, N. (2012). *Geological study of Triassic reservoirs in the province of Noord-Brabant*. <https://doi.org/10.1016/B978-0-12-801027-3.00011-7>
- McKie, T. (2017). Paleogeographic Evolution of Latest Permian and Triassic Salt Basins in Northwest Europe. In *Permo-Triassic Salt Provinces of Europe, North Africa and the Atlantic Margins* (pp. 159–173). Elsevier. <https://doi.org/10.1016/B978-0-12-809417-4.00008-2>
- Miall, A. D. (1985). Architectural-element analysis: a new method of facies analysis applied to fluvial deposits. In *Recognition of Fluvial Depositional Systems and Their Resource Potential (SC19)* (pp. 33–81).
- Nelskamp, S., & Verweij, J. M. (2012). Using basin modeling for geothermal energy exploration in the Netherlands -an example from the West Netherlands Basin and Roer Valley Graben, 113.
- Pallatt, N., Wilson, J., & McHardy, B. (1984). The Relationship Between Permeability and the Morphology of Diagenetic Illite in Reservoir Rocks. *Journal of Petroleum Technology*, 36(12), 2225–2227. <https://doi.org/10.2118/12798-PA>

Partner Workshop K18-Golf Unit - Sedimentology & Reservoir Quality. (2016).

- Pluymaekers, M. P. D., Kramers, L., van Wees, J.-D., Kronimus, A., Nelskamp, S., Boxem, T., & Bonté, D. (2012). Reservoir characterisation of aquifers for direct heat production: Methodology and screening of the potential reservoirs for the Netherlands. *Netherlands Journal of Geosciences*, *91*(4), 621–636. <https://doi.org/10.1017/S001677460000041X>
- Rafik, B., & Kamel, B. (2017). Prediction of permeability and porosity from well log data using the nonparametric regression with multivariate analysis and neural network, Hassi R'Mel Field, Algeria. *Egyptian Journal of Petroleum*, *26*(3), 763–778. <https://doi.org/10.1016/j.ejpe.2016.10.013>
- Ramm, M. (2000). Reservoir quality and its relationship to facies and provenance in Middle to Upper Jurassic sequences, northeastern North Sea. *Clay Minerals*, *35*, 77–77. <https://doi.org/10.1180/000985500546747>
- Rider, M. H. (1990). Gamma-ray log shape used as a facies indicator: critical analysis of an oversimplified methodology. *Geological Society, London, Special Publications*, *48*(1), 27–37. <https://doi.org/10.1144/GSL.SP.1990.048.01.04>
- Rogers, S. J., Fang, J. H., Karr, C. L., & Stanley, D. A. (1992). Determination of lithology from well logs using a neural network. *The American Association of Petroleum Geologists Bulletin*, *76*(5), 731–739.
- Serra, O. E. (1983). *Fundamentals of well-log interpretation*.
- Slatt, R. M. (2013). Geologic controls on reservoir quality. In *Stratigraphic Reservoir Characterization for Petroleum Geologists, Geophysicists, and Engineers* (Vol. 61, pp. 229–281). <https://doi.org/10.1016/B978-0-444-56365-1.00006-7>
- Sneider, R. M. (1987). Practical petrophysics for exploration and development. In *American Association of Petroleum Geologists Short Course Lecture Notes* (p. variously paginated).
- Ursem, B. N. A. (2018). *Relating Main Buntsandstein paleo-environments to present-day porosities in the West Netherlands Basin: An integrated study of core, wireline, and seismic data*. Utrecht University.
- van Kempen, B. M. M., Mijnlief, H. F., & van der Molen, J. (2018). Data mining in the Dutch Oil and Gas Portal: a case study on the reservoir properties of the Volpriehausen Sandstone interval. *Geological Society, London, Special Publications*, *469*, SP469.15. <https://doi.org/10.1144/SP469.15>
- van Wees, J. D., Stephenson, R. A., Ziegler, P. A., Bayer, U., McCann, T., Dadlez, R., ... Scheck, M. (2000). On the origin of the southern Permian Basin, Central Europe. *Marine and Petroleum Geology*, *17*(1), 43–59.
- Vis, G.-J., Van Gessel, S. F., Mijnlief, H. F., Pluymaekers, M. P. D., Hettelaar, D. P. M., & Stegers, D. P. M. (2010). Lower Cretaceous Rijnland Group aquifers in the West Netherlands Basin : suitability for geothermal, 55.
- Vissers, R. L. M. (2012). Extension in a convergent tectonic setting: a lithospheric view on the Alboran system of SW Europe. *Geologica Belgica*, *15*, 53–72. Retrieved from <http://cat.inist.fr/?aModele=afficheN&cpsid=25670264>
- Vogel, M. A., & Wong, A. K. C. (1979). PFS clustering method. *IEEE Transactions on Pattern Analysis and Machine Intelligence, PAMI-1*(3), 237–245. <https://doi.org/https://doi.org/10.1109/TPAMI.1979.4766919>
- Winstanley, A. M. (1993). A review of the Triassic play in the Roer Valley Graben, SE onshore Netherlands. In *Petroleum Geology of Northwest Europe: Proceedings of the 4th Conference* (Vol. 4, pp. 595–607). Geological Society of London. <https://doi.org/10.1144/0040595>
- Wong, P. M., Jian, F. X., & Taggart, I. J. (1995). A critical comparison of neural networks and discriminant analysis in lithofacies, porosity and permeability predictions. *Journal of Petroleum Geology*, *18*(2), 191–206.
- Zijerveld, L., Stephenson, R., Cloetingh, S., Duin, E., & van den Berg, M. W. (1992). Subsidence analysis and modelling of the Roer Valley Graben (SE Netherlands). *Tectonophysics*, *208*(1–3), 159–171. [https://doi.org/10.1016/0040-1951\(92\)90342-4](https://doi.org/10.1016/0040-1951(92)90342-4)

Websites:

NLOG.nl

Appendix I: Glossary/Index

Logs

GR	Gamma ray log
RHOB	Bulk density log
NPHI	Neutron porosity log
DT	Sonic log
RESD	Resistivity log
Sw	Water saturation log
CALI	Caliper log

Stratigraphy

RN	Upper Germanic Trias Group
RNROF	Röt Fringe Sandstone Member
RNROY	Upper Röt Fringe Claystone Member
RB	Lower Germanic Trias Group
RBMVU	Upper Volpriehausen Sandstone Member
RBMVL	Lower Volpriehausen Sandstone Member
RBMDU	Upper Detfurth Sandstone Member
RBMDL	Lower Detfurth Sandstone Member

Structural elements

RVG	Roer Valley Graben (Roerdalslenk)
RM	Rhenish Massif
LBM	London Brabant Massif
WNB	West Netherlands Basin

Wells

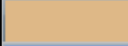
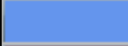



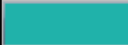
KDK-01	Keldonk
BRAK-01	Brakel
WWK-01	Waalwijk
WWS-01-S1	Waalwijk Zuid, sidetrack 1
WWN-01-S2	Waalwijk Noord, sidetrack 2
NDW-01	Nederweert

Other

MB	Maximum burial depth
BA	Burial anomaly
PDF	Probability Density Function
PSF	Pseudo-F Statistic
ϕ	Porosity
PHI	Porosity
PHIE	Effective porosity
k	Permeability
RMS	Root mean square



Appendix II: Depositional environments

The following depositional settings were used as the input for facies classification. The lithological logs from the studies are all open for access via NLOG.nl. Depositional settings of a comparable nature have been merged. The facies sequences from the cores have been described downwards.

Name	Background
Sheetfloods	 ▼
Fluvial channel	 ▼
Floodplain pond	 ▼
Abandoned channel/overbank	 ▼
Braided channel complex	 ▼
Floodplain with minor fluvial channels	 ▼

BRAK-01

Interpretation derived from lithological log by F. de Reuver, GAPS Nederland B.V., October 1992.

BRAK-01: upper interval: 2349 – 2369,10 mBRT	
Depositional settings: <ol style="list-style-type: none"> 1. Fluvial channel 2. Sheetflood 3. Fluvial channel 4. Sheetfloods with minor channeling/scouring 5. Floodplain pond/lake with influence of sheetfloods Floodplain pond/lake 	
BRAK-01: lower interval: 2452 – 2478.65 mBRT	
Depositional settings: <ol style="list-style-type: none"> 1. Floodplain pond/lake influenced by sheetfloods 2. Sheetfloods with minor channeling 3. Ephemeral floodplain pond / abandoned channel fill 4. Braided channel complex 5. Floodplain pond/lake 6. Sheetfloods with minor channeling 7. Ephemeral floodplain pond/lake 8. Homogenized sheetfloods in floodplain pond/lake (?) 9. Shallow ephemeral floodplain pond 10. Stacked sheetfloods 11. Floodplain pond 	

KDK-01




Interpretation derived from lithological log by F. de Reuver, GAPS Nederland B.V., July 1992.

KDK-01: upper interval: 1944 – 1981 mBRT	
Depositional settings: 1. Floodplain pond/lake 2. Sheetfloods Floodplain with ponds/lakes and minor channels and minor soils 3. Abandoned channel? Overbank? 4. Braided channel complex 5. Floodplain 6. Sheetfloods (distal alluvial fan?)	
KDK-01: lower interval: 2258 – 2275,10 mBRT	
Depositional settings: 12. Braided channel complex 13. Floodplain with minor fluvial channels	

WWN-01-S2

Interpretation derived from lithological log by C.Cade, BP Exploration, July 1989.

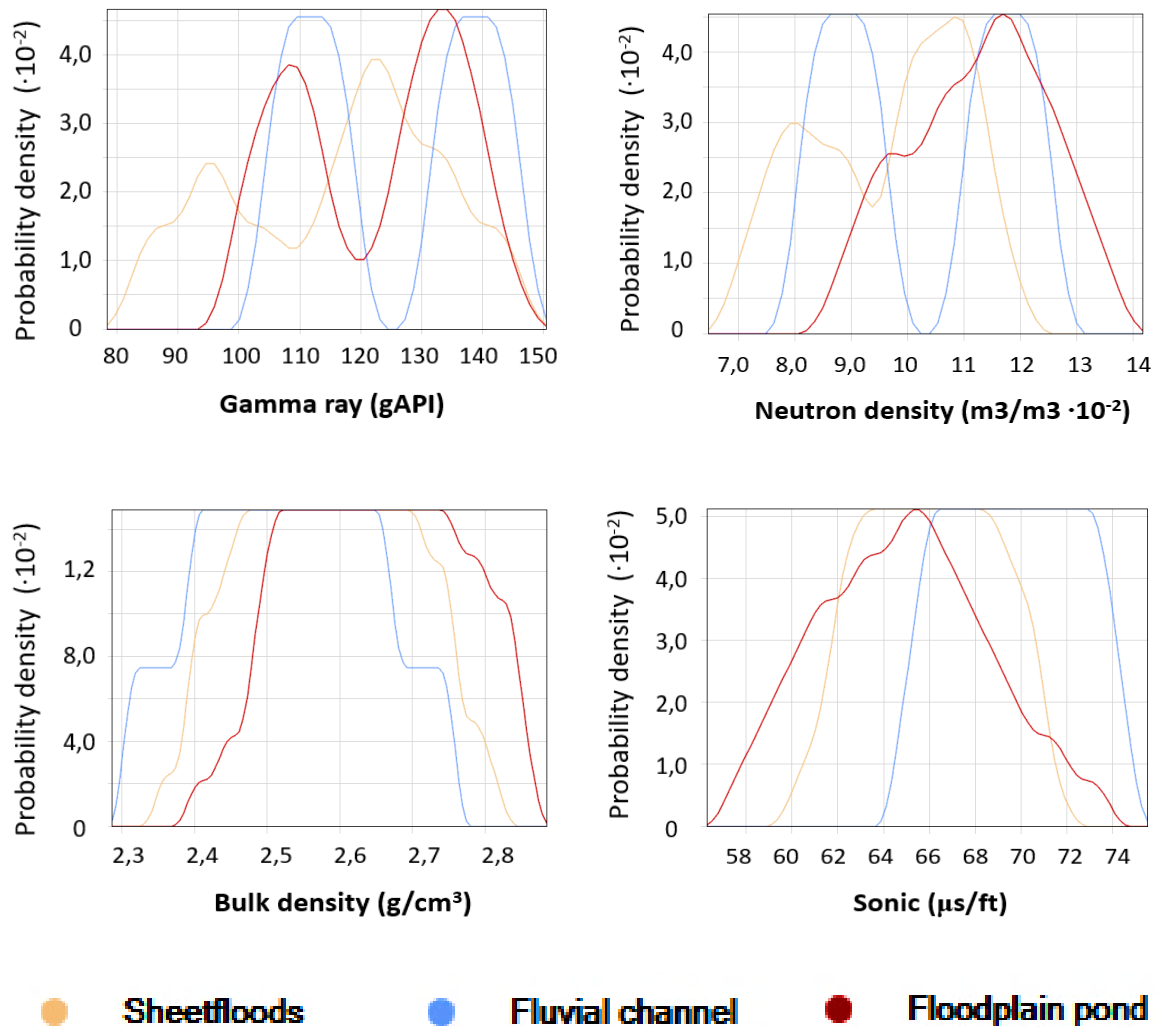
WWN-01-S2: 3169 – 3305 mBRT		
Core 3	Depositional settings: 1. Stacked streamflood Channel plug/mudflat Amalgamated streamflood sequence Floodplain with dolocrete Streamflood Sheetflood Channel + minor mudflat sequence Streamflood/sheetflood complex Stacked channel sequence Streamflood Stacked channel sequence Stacked streamflood complex Sheetflood Stacked streamflood sequence with local dolocretes 2. Floodplain sequence 3. Stacked streamflood complex	
Core 4	1. Stacked streamflood complex with localized dolocrete Amalgamated sheetflood complex Stacked streamflood complex Sheetflood 2. Channel/streamflood complex Mudflat/channel plug	

Core 5	<ol style="list-style-type: none"> 1. Stacked channel complex 2. Stacked streamflood complex local minor sheetfloods 3. Stacked streamflood complex with minor channels 4. Stacked channel sequence 	
Core 6	<ol style="list-style-type: none"> 1. Stacked sheetfloods Streamflood 2. Channel/minor streamflood sequence with local mudflat development Stacked channel sequence 3. Amalgamated streamfloods Streamfloods Stacked sheetflood complex 4. Channel complex Streamflood/minor channel 	
Core 7	<ol style="list-style-type: none"> 1. Heterolithic floodplain sequence 2. Streamflood 3. Stacked channel complex 4. Stacked sheetflood complex 5. Channel complex 6. Stacked sheetflood and minor streamflood complex with local minor channels and rare mudflats 	

Appendix III: Results Lithoclassification Petrel

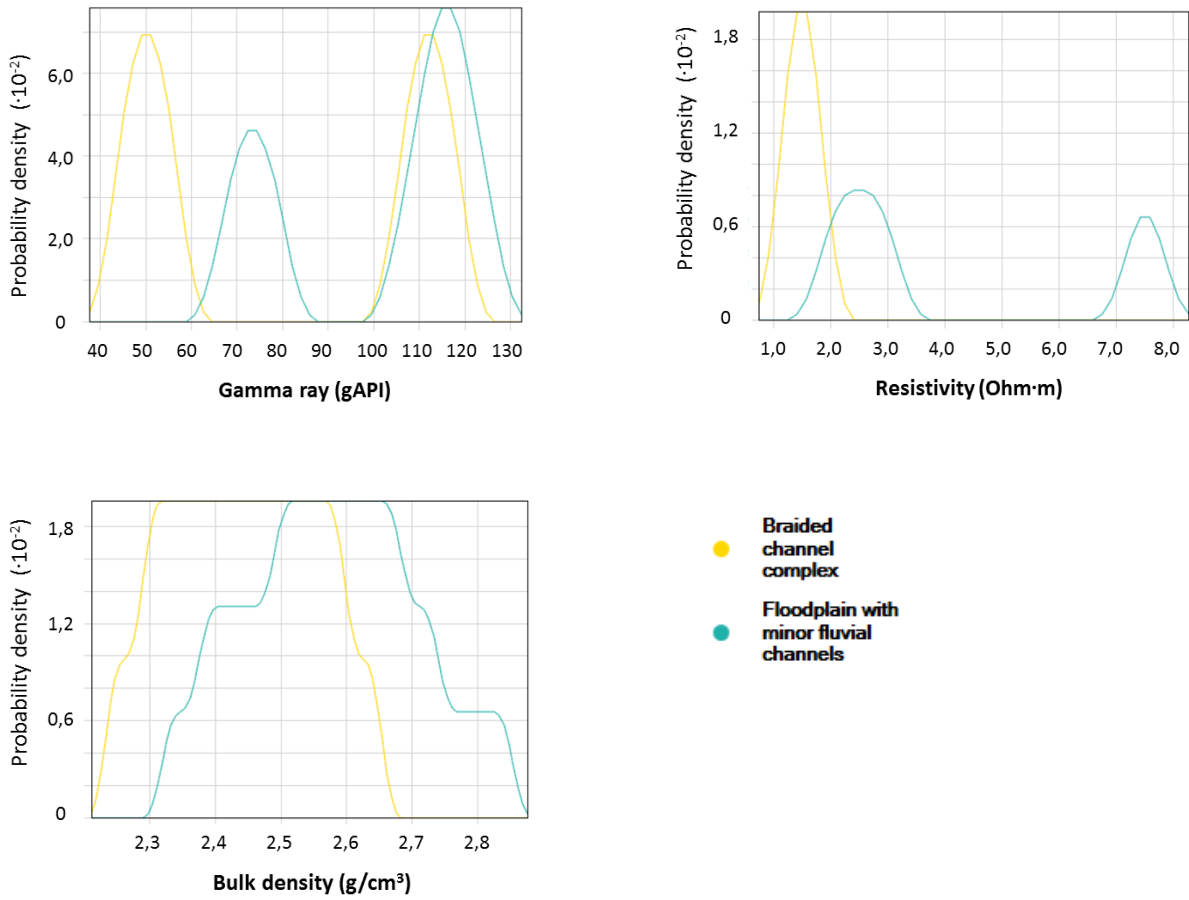
Probability density functions (PDFs)

BRAK-01



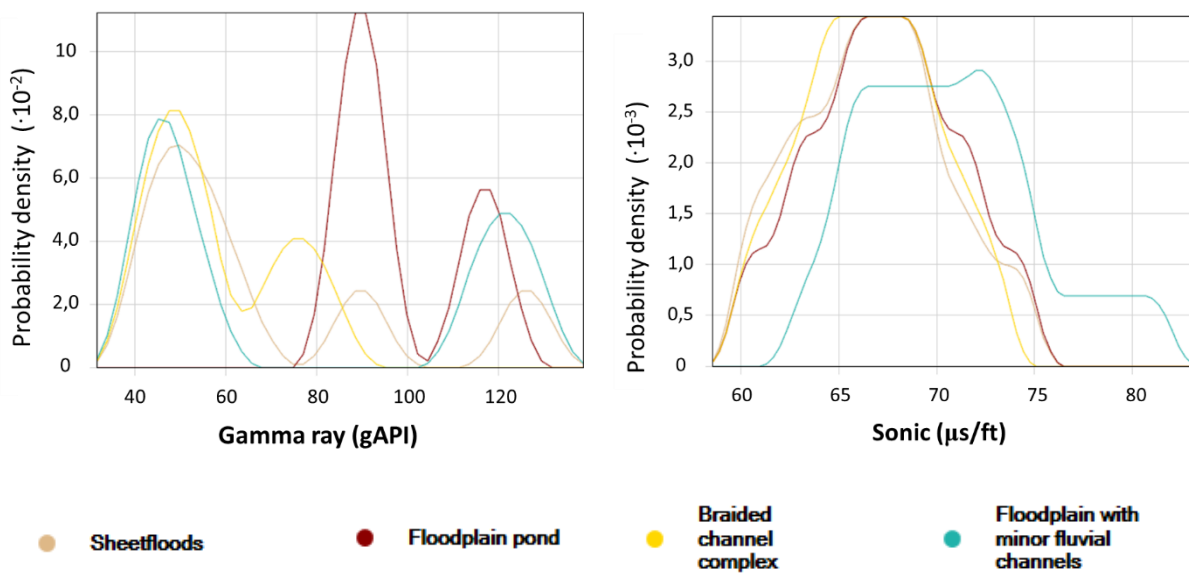
Probability density functions for BRAK-01.

KDK-01



Probability density functions for KDK-01.

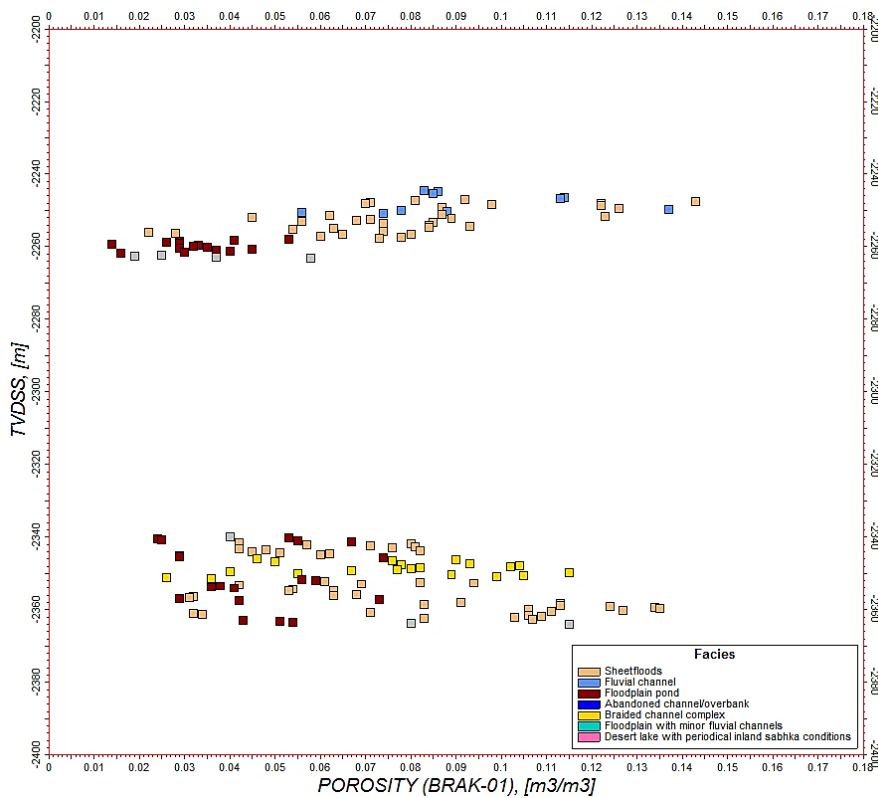
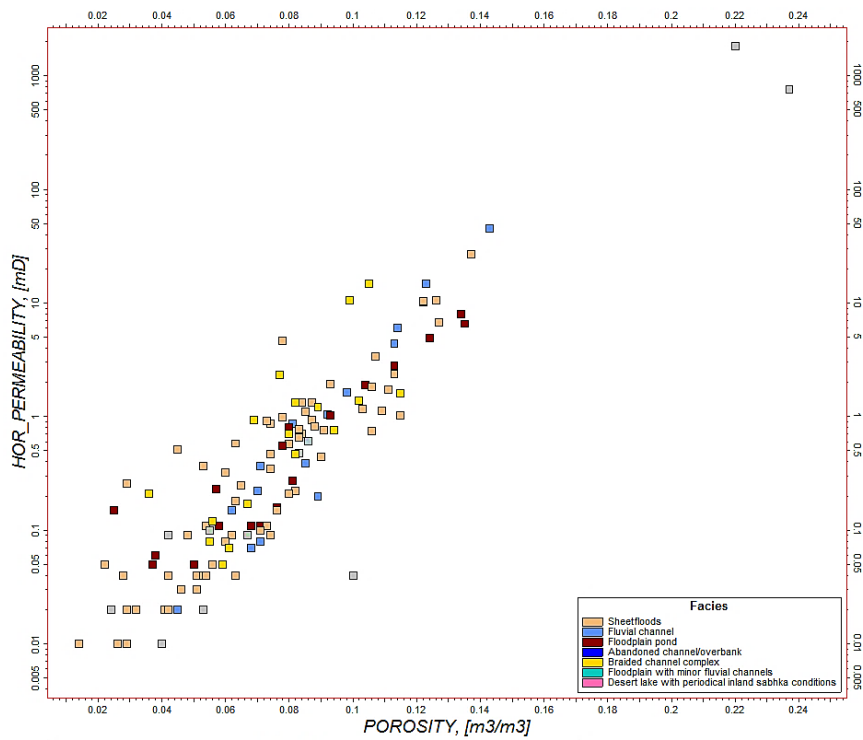
WWN-01-S2



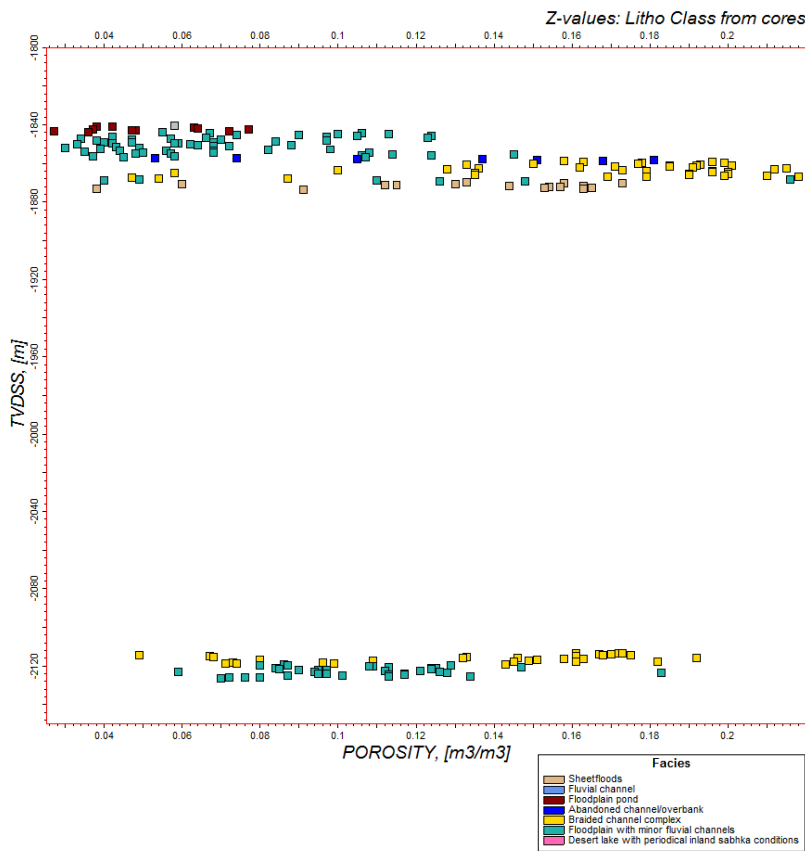
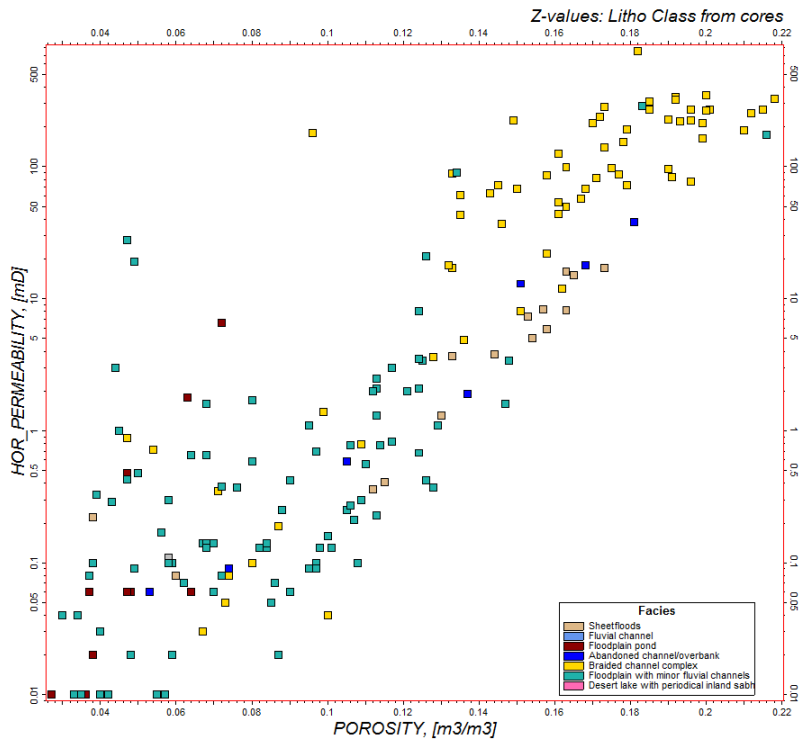
Probability density functions for WWN-01-S2.

Poroperms & porosity-depth plots

BRAK-01

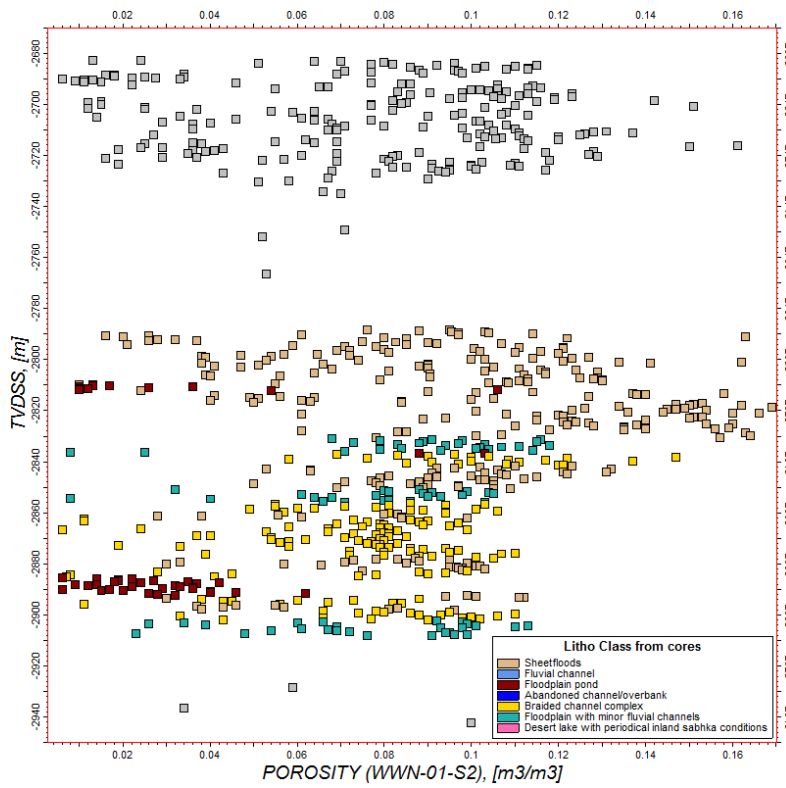
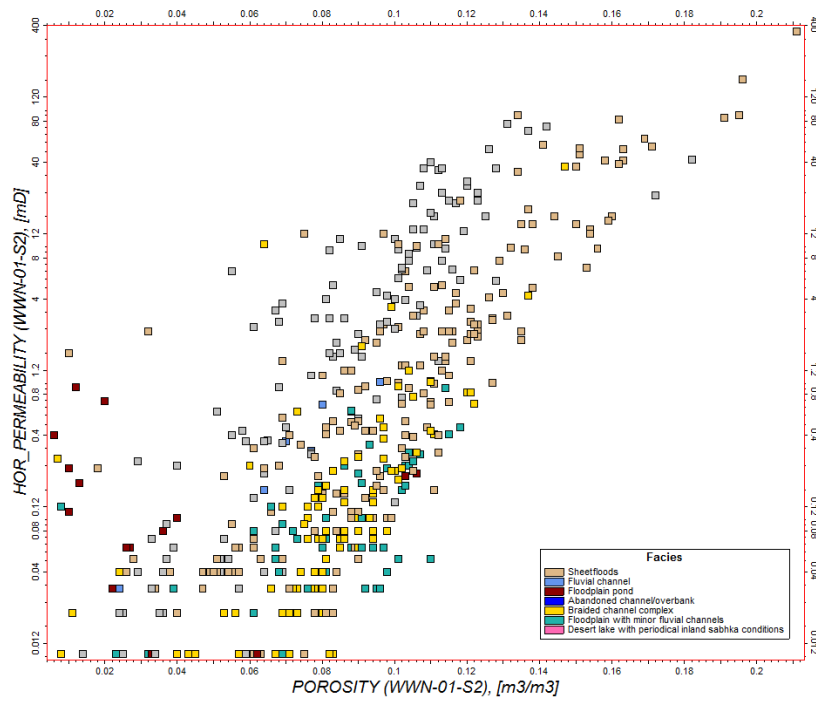


Results from lithoclassification in Petrel based on a neural net. (A): Poroperm from BRAK-01. (B): Porosity-depth plot from BRAK-01.



Results from lithoclassification in Petrel based on a neural net. (A): Poroperm from KDK-01. (B): Porosity-depth plot from KDK-01.

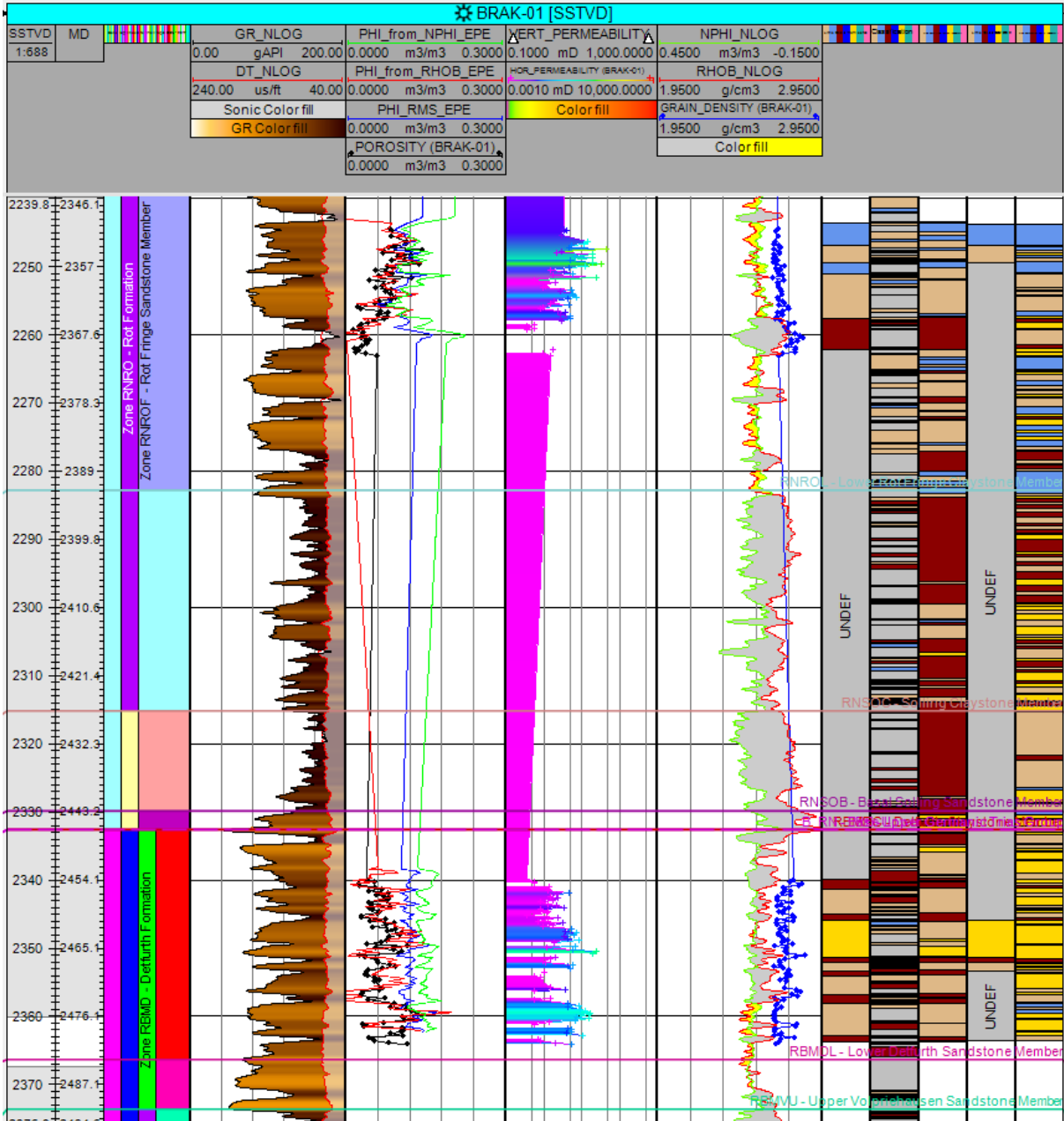
WWN-01-S2

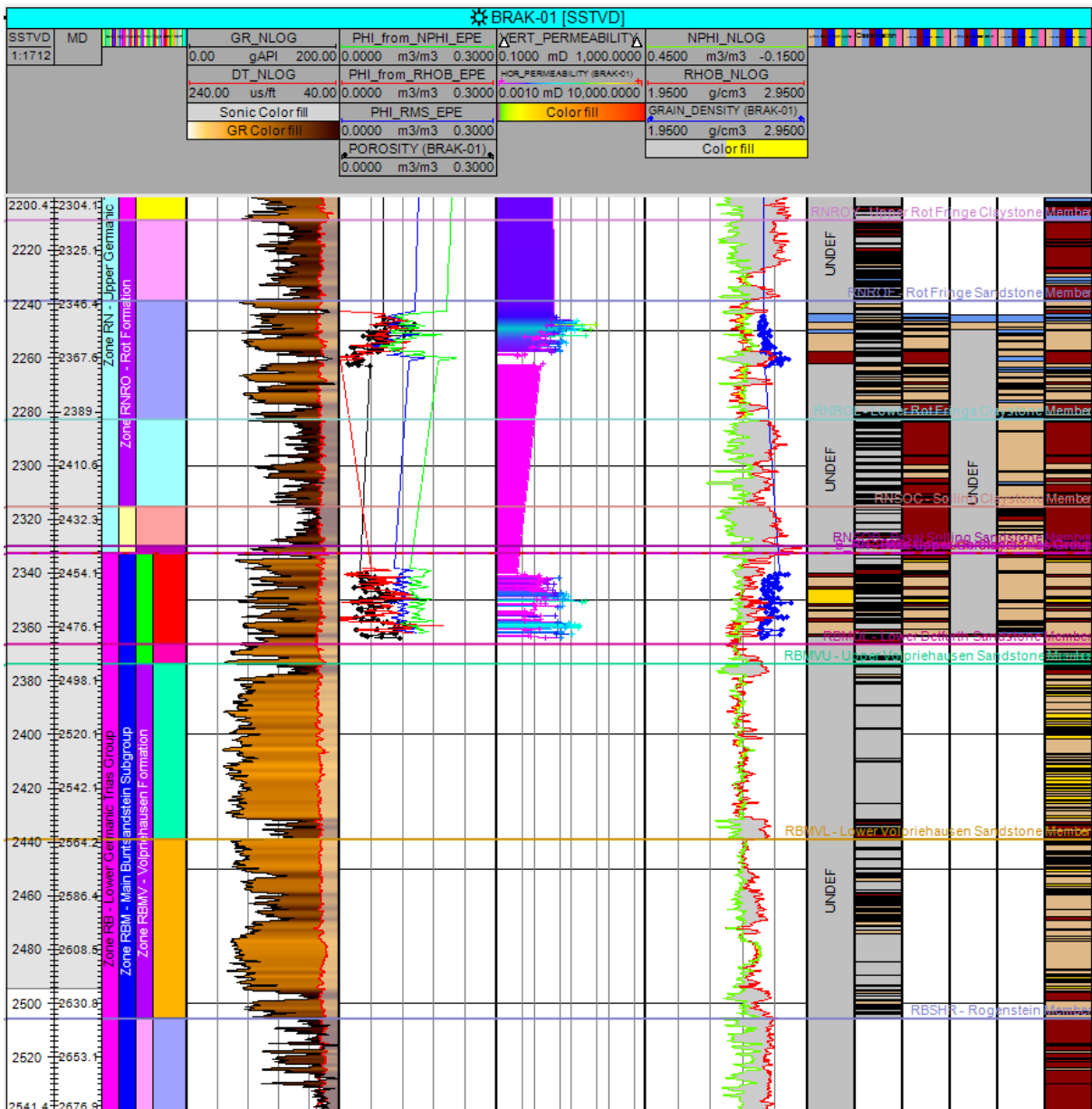


Results from lithoclassification in Petrel based on a neural net. (A): Poroperm from WWN-01-S2. (B): Porosity-depth plot from WWN-01-S2.

Appendix IV: Well sections

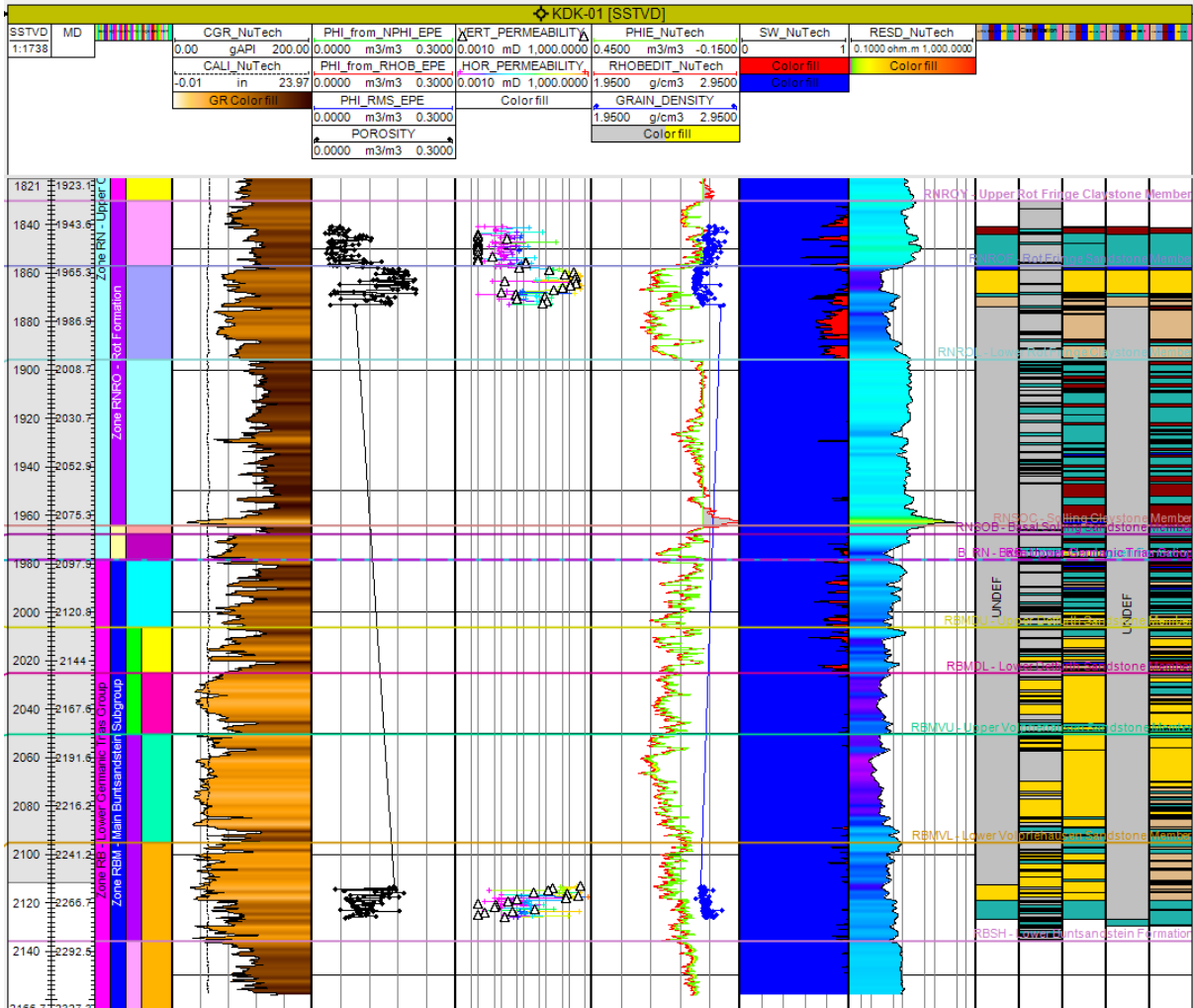
BRAK-01



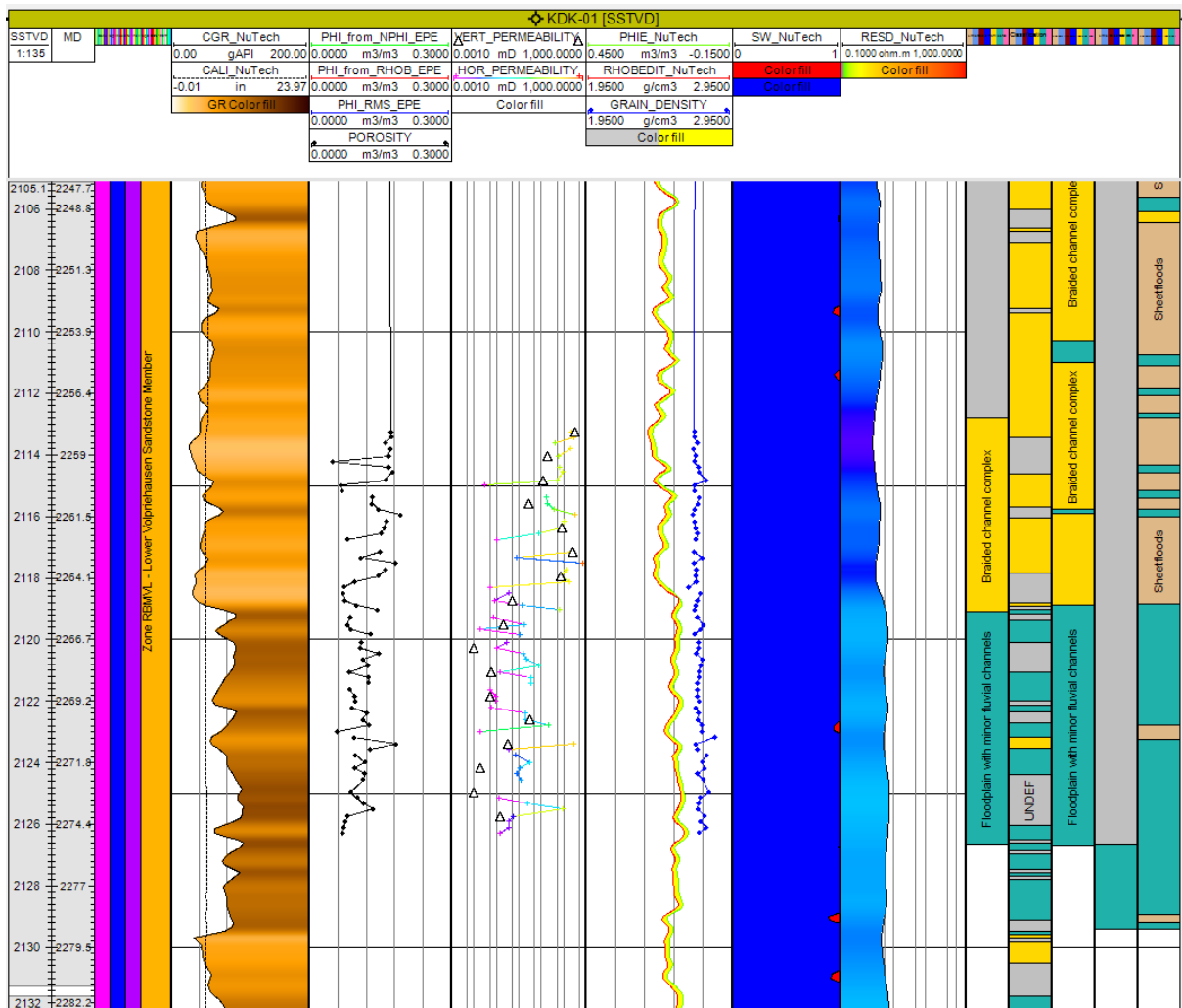


Extended well section of BRAK-01 from Petrel including the lithoclassification input and results. The last panel shows the neural net prediction over a larger well interval.

KDK-01

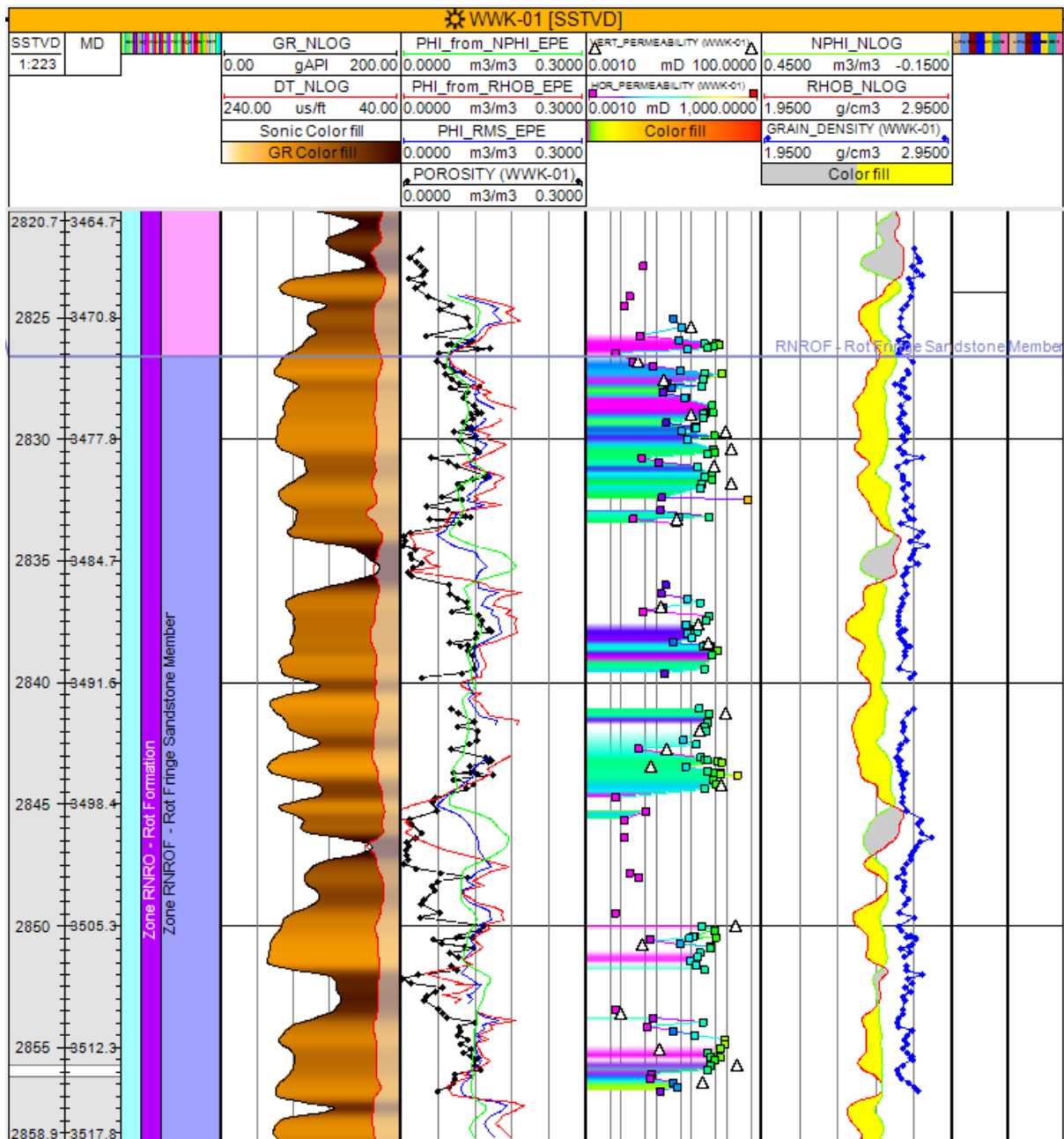


Well section of KDK-01 from Petrel including the lithoclassification input and results.



Close-up of the Petrel well section of BRAK-01 with the lithoclassification input and results.

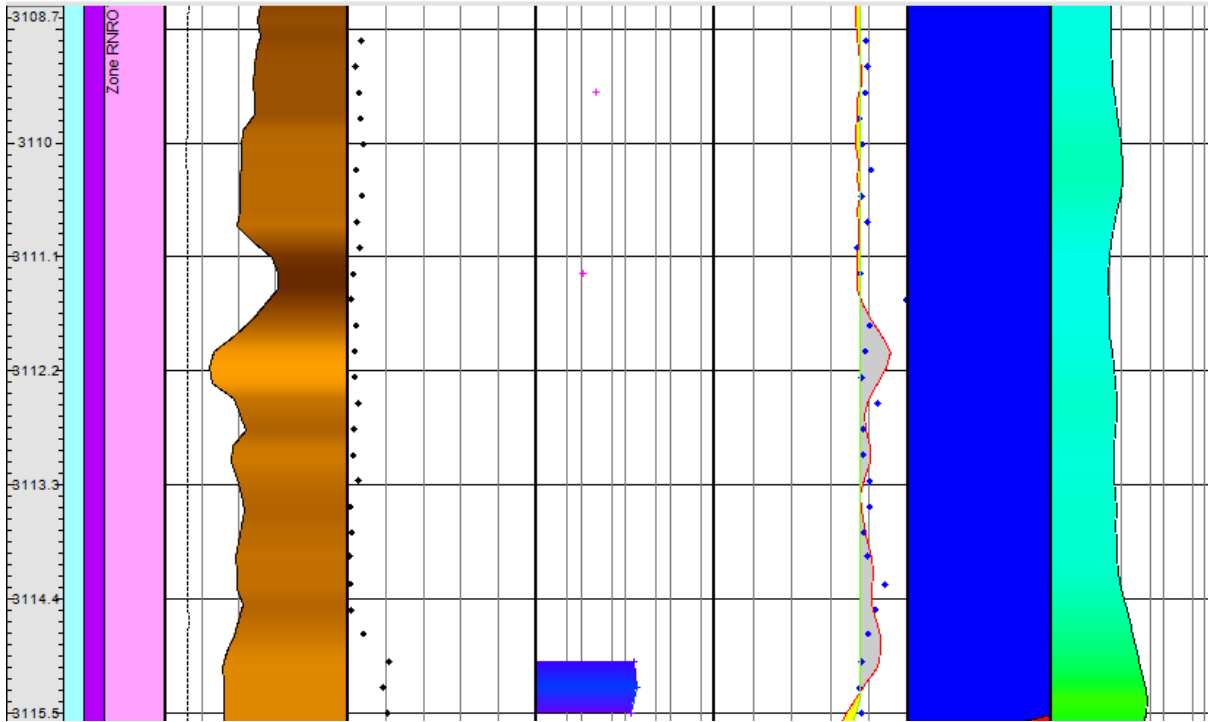
WWK-01



Well section of WWK-01 from Petrel.

WWS-01-S1

WWS-01-S1 (SSTVD)						
MD	CGR_NuTech	PHI_from_NPHI_EPE	XERT_PERMEABILITY	PHIE_NuTech	SW_NuTech	RESD_NuTech
	0.00 gAPI 200.00	0.0000 m3/m3 0.3000	0.1000 mD 1,000.0000	0.4500 m3/m3 -0.1500	0	1.0000 ohm.m 1,000.0000
	CAL1_NuTech	PHI_from_RHOB_EPE	HOR_PERMEABILITY	RHOBEDIT_NuTech	Color fill	Color fill
	6.95 in 20.24	0.0000 m3/m3 0.3000	0.0010 mD 100.0000	1.9500 g/cm3 2.9500	Color fill	
	GR Color fill	PHI_RMS_EPE	Color fill	GRAIN_DENSITY		
		0.0000 m3/m3 0.3000		1.9500 g/cm3 2.9500		
		POROSITY		Color fill		
		0.0000 m3/m3 0.3000				



Well section of WWS-01-S1 from Petrel.

